The Global Gravity-based Groundwater Product (G3P)

Andreas Güntner[1,2], Ehsan Sharifi[3,1], Julian Haas[1], Eva Boergens[1], Feifei Cao[8], Christoph Dahle[1], Neda Darbeheshti[6,9], Henryk Dobslaw[1], Inés Dussaillant[7], Wouter Dorigo[5], Frank Flechtner[1], Adrian Jäggi[6], Miriam Kosmale[4], Martin Lasser[6], Kari Luojus[4], Ulrich Meyer[6], Adam Pasik[5], Wolfgang Preimesberger[5], Claudia Ruz Vargas[8], Michael Zemp[7]

[1]GFZ Helmholtz Centre for Geosciences, Potsdam, 14473, Germany
[2]University of Potsdam, Institute of Environmental Science and Geography, Potsdam, 14476, Germany
[3]Institute of Meteorology and Climate Research-Troposphere Research (IMK-TRO), Karlsruhe Institute of Technology (KIT), Karlsruhe, 76131, Germany
[4]Finnish Meteorological Institute, FMI, Arctic Space Center, Helsinki, 00560, Finland
[5]TU Wien, Department of Geodesy and Geoinformation, Vienna, 1040, Austria
[6]University Bern, Astronomical Institute, Bern, 3012, Switzerland
[7]Department of Geography, University of Zurich, Zurich, 8057, Switzerland
[8]International Groundwater Resources Assessment Centre IGRAC, Delft, Netherlands
[9]Geoscience Australia, Canberra, Australia

Correspondence to: Andreas Güntner (andreas.guentner@gfz.de)

Abstract. Groundwater is one of the most important freshwater resources for ecosystems and mankind. Because of its fundamental role in the Earth's water and energy cycles, groundwater has been declared an essential climate variable by GCOS, the Global Climate Observing System. Similar to other subsurface states and fluxes, groundwater is difficult to monitor at the global scale, with sufficient spatial coverage and over climate-relevant time scales. The Global Gravity-based Groundwater Product (G3P) is a global observation-based data set of large-scale groundwater storage variations. G3P capitalizes on the unique capability of GRACE and GRACE-FO satellite gravimetry as the only remote sensing technology to monitor subsurface mass variations. In a mass balance approach, satellite-based, in situ observation-based and model-based water storage variations of snow water equivalent, root-zone soil moisture, glacier mass, and surface water storage are subtracted from GRACE/-FO terrestrial water storage anomalies to result in monthly variations of groundwater storage. For this combination, the individual compartmental storage data are spatially filtered to be consistent with the spatial resolution of terrestrial water storage from satellite gravimetry. The G3P data set presented here covers the period 2002 to 2023 with monthly resolution on a 0.5° global grid and includes propagated uncertainty information. We describe the details of the G3P data processing chain and of each contributing data stream, provide examples of spatial and temporal groundwater storage variations represented by the G3P data set, and present exemplary evaluation results against in situ groundwater observations for three large aquifer systems. The latter show moderate to high temporal correlation of aquifer-average G3P groundwater storage and in situ groundwater level variations on seasonal and interannual time scales. G3P is a prototype for an operational global groundwater

service, under development as a cross-cutting extension of the existing portfolio of the Copernicus Climate Change Service C3S. The G3P data set is available via GFZ Data Services at https://doi.org/10.5880/G3P.2024.001 (Güntner et al., 2024).

Short summary. We provide a data set that illustrates how the amount of water that is stored in the subsurface as groundwater varies in time over the continents of the Earth. An important part of the data comes from satellites that track changes in water by its gravity effect. The data allow for assessing how groundwater as the most important freshwater resource for mankind and ecosystems is affected by climate variability, climate change and withdrawal by human activities.

1 Introduction

Groundwater is water in the subsurface that completely fills the pore spaces, voids or fractures of the soil and rock under water-saturated conditions. This makes it different from water storage under unsaturated conditions in the vadose zone, including soil moisture. Groundwater storage is recharged by infiltration and percolation of precipitation, snow and glacier melt and surface water, while losses are due to discharge to continental surface water bodies and to the ocean, evapotranspiration, and groundwater withdrawal. It typically responds in a delayed and smoothed way to the hydro-meteorological dynamics at the Earth surface. Residence times and ages of groundwater can vary over several orders of magnitude depending on the climate and hydrogeological conditions and on its depth below the surface, with groundwater recharged over the last few decades making up a small fraction of the total groundwater volumes on Earth only (Gleeson et al., 2016). The sensitivity of groundwater dynamics to climate variability is characterized by hydraulic memory effects that vary spatially with the environmental conditions (Opie et al., 2020; Cuthbert et al., 2019). Climate change and human activities have caused major changes to groundwater processes, fluxes and storage dynamics at the global scale during recent decades (Kuang et al., 2024). Groundwater is an important indicator of how climate variability and change impact the global hydrological cycle. In turn, groundwater-driven feedback on the climate system is prevalent through groundwater-dependent ecosystems in riparian, wetland or deep-rooted habitats (Taylor et al., 2013; Saccò et al., 2024). Against this background, the Global Climate Observing System (GCOS) declared groundwater an Essential Climate Variable (ECV) (Bojinski et al., 2014), represented by the ECV quantities groundwater storage change and groundwater level (Wmo, 2022). Uncertainties in estimating long-term trends of groundwater storage due to the limited spatial coverage, resolution or record length of groundwater observations and due to natural inter-annual climate variability need to be considered (Shamsudduha and Taylor, 2020). In many regions worldwide, though, the environmental changes and human impacts have led to a depletion of aquifers and declining groundwater levels in recent decades (for example, California's Central Valley, aquifers in Iran, on the Arabian Peninsula, or in the Indian subcontinent). At the same time, there are also noticeable exceptions where negative trends could be reversed following management changes (for example, the Bangkok basin, the Upper Santa Cruz basin in the U.S., the North China Plain) (e.g., Jasechko et al. (2024), Chandanpurkar et al. (2025), Bierkens and Wada (2019), Long et al. (2025)). The already existing and the projected shortage of groundwater availability as the primary water resource for many regions worldwide are

urging for management strategies towards sustainable and resilient water systems (e.g., Karandish et al. (2025), Scanlon et al. (2023)).

In view of the prominent role of groundwater outlined above, its analysis and assessment within a holistic Earth system and socio-ecological framework requires global-scale, observation-based groundwater-related data sets. However, their availability, relevance, timeliness, or unbiasedness are facing many limitations (Huggins et al., 2025). In terms of groundwater volumes, the standard approach for characterizing its spatio-temporal dynamics is by in situ observations in boreholes or wells in which the groundwater level is recorded continuously by, e.g., pressure sensors, or manually at selected points in time. Many countries operate national groundwater monitoring networks. Optimizing the design of a network requires a thorough understanding of the local and regional hydrogeological conditions and advanced regionalization methods (e.g., Hosseini and Kerachian (2017)). As setting up and maintaining the networks is costly, in situ-based groundwater records are often sparse, short or discontinuous. Restrictive data sharing policies further reduce the number of accessible data sets. The Global Groundwater Monitoring Network (GGMN) (https://ggis.un-igrac.org/view/ggmn/), as a network of networks, connects national services and provides today the only global dataset of groundwater levels. Converting the observed head variations into groundwater volume, i.e., storage variations at the aquifer or regional scale, involves considerable uncertainty from poorly known storage coefficients or specific yield values, from local site-specific groundwater dynamics, and possible biases from management-driven clustering of observation wells in highly productive aquifers.

At the global scale, the Gravity Recovery and Climate Experiment (GRACE) satellite mission (Tapley et al., 2004) and its successor GRACE Follow-On (GRACE-FO) (Landerer et al., 2020) map the Earth's gravity field since April 2002 with usually monthly resolution. The observed temporal variations of the gravity field are caused by mass changes on and below the Earth surface, with variations of terrestrial water storage (TWS) being the dominant mass change component on the continents after removing mass effects of the atmosphere, the ocean and from geodynamic processes, i.e., glacial isostatic adjustment or megathrust earthquakes. Other non-hydrological mass changes, such as erosion and sediment transport, mining, exploitation of fossil fuels, or vegetation and related biomass changes, are usually neglected because their magnitude is too small to be sensed with the current gravimetric technology in orbit. As satellite gravimetry does not determine the absolute value of TWS but its temporal variations, it is common practice to express the data as TWS anomalies (TWSA) relative to an arbitrary long-term mean. TWS is an integrative hydrological state variable that encompasses various water storage compartments (WSCs) of the continental hydrological cycle, including water storage as soil moisture in the unsaturated zone (UZS), snow cover in the form of snow water equivalent (SWE), the mass of glaciers (GM) and ice sheets (ISM), storage in surface water bodies such as rivers, lakes and reservoirs (SWS), and groundwater. Thus, GRACE/-FO observations provide a unique means of quantifying groundwater storage anomalies (GWSA) at large spatial scales. This is achieved by subtracting the storage anomalies A of all compartments other than groundwater from TWSA, following a water budget approach (Eq. 1) (Güntner et al., 2007).

$$GWSA = TWSA - A(UZS + SWE + GM + ISM + SWS) \quad (1)$$

This approach has been used in numerous studies for selected large aquifers, regions or countries, and for some global-scale analyses, illustrating groundwater dynamics driven by climate variability, human groundwater use and other drivers (see reviews by Chen et al. (2016), Frappart and Ramillien (2018), Springer et al. (2023), Adams et al. (2022)). Also, data assimilation frameworks (e.g., Li et al. (2019)) and offline data mering approaches (e.g., Mehrnegar et al. (2021),Van Dijk et al. (2014)) were used for isolating GWSA from TWSA. Several combinations to solve Eq. (1) by using model outputs, remote-sensing observations or in situ observations to quantify the required WSC anomalies have been carried out. The large majority of studies used simulated WSC data of hydrological or land-surface models. For water storage in the unsaturated zone, usually simulated near-surface soil moisture down to 1 or 2 meters below the Earth surface is used, often also referred to as root zone soil moisture (RZSM). Nearly every gravity-based GWSA study used its individual (combination of) sources for the GRACE/-FO and WSC data sets. Depending on the study and its region of interest, some WSCs were discarded as they were considered to be negligible components of the hydrological cycle in that area. Akl and Thomas (2024) highlight the considerable inconsistencies and uncertainties that arise for GWSA due to the choice of the individual storage data sets among GRACE/-FO-based TWSA products from different processing centres, and among model-based WSCs from different hydrological models. The latter differ from each other depending on model structure, parameters and forcing data, for instance. Also Getirana et al. (2025) and Arifin et al. (2025) recently point out the uncertainties of GWSA obtained with the water budget approach and model-based storage terms and that careful interpretation and evaluation is needed. Other limitations and uncertainties in the resulting GWSA are due to the coarse spatial resolution of GRACE/-FO data (>200 km) that also encompasses signal leakage. Leakage can lead to spurious mass change in the region of interest that originates from adjacent areas. It is caused by the particular technology of satellite gravimetry where the observed gravity acceleration cannot be attributed uniquely to a certain area of origin on or below the Earth Earth's surface. Furthermore, uncertainties and errors originate from spatial smoothing and the removal of real TWSA signals by filtering of GRACE-/FO satellite data. This filtering is necessary to reduce instrumental and processing noise and temporal aliasing effects induced by high-frequency variations of atmospheric and oceanic mass variations, e.g., Shihora et al. (2022). In this context, the existing gravity-based GWSA studies also vary in the way of data pre-processing to make the different data sets compatible before applying the subtraction of Eq. (1). This includes in particular the approach for spatial alignment such as GRACE-like spatial filtering or the application of scaling factors (e.g., Landerer and Swenson (2012), Long et al. (2015)) that some studies apply to restore signals that may have been suppressed by data filtering. Substantial methodological differences are also found in the uncertainty quantification for the resulting GWSA data.

In this work, we introduce the Global Gravity-based Groundwater product (G3P). The purpose is to provide a global-scale data set of temporal and spatial variations of groundwater storage that is consistently processed over the entire continental domain, including all relevant water storage compartments. The data set shall serve as the basis for an observation-based, stable and frequently extended climate data record for the ECV groundwater. It shall be applicable for performing a multitude of water cycle and water resources analyses in the context of global change processes, such as those addressed in the previous paragraphs.

2 Data and methods

2.1 G3P general concept

G3P follows the water budget approach outlined in Eq. (1). Monthly GWSA are quantified by subtracting the monthly storage anomalies of all other WSCs of the continental water cycle from the integrative water mass variations observed by satellite gravimetry, i.e., GRACE/-FO-based TWSA. Different from other studies, the G3P approach strives for observation-based products for all involved data sets. This was motivated by, first, providing a climate data record that is mostly observation-driven and therefore as independent as possible from global model outputs and, secondly, developing a cross-cutting product that builds on existing observation-based climate data records available through Copernicus services. As detailed in Sect. 2.2, observation-based data sets besides TWSA are used in particular for soil moisture, snow storage and glacier mass changes, derived independently from satellite gravimetry, from remote sensing and in situ monitoring. G3P excludes Greenland and Antarctica and, hence, does not consider mass changes of these two ice sheets (ISM in Eq. (1)). The only fully model-based WSC used in the current version of G3P is surface water storage.

The G3P processing chain from the individual input data sets to the GWSA product is depicted in Fig. 1. TWSA from GRACE/-FO and storage data sets of the individual WSCs are provided with respective uncertainty estimates and need to be resampled to a common global grid (resolution of 0.5° in the case of G3P) and masked with the same land-ocean mask (see Sect. 2.3.1 and 2.3.2). Due to the measurement principle and the necessary data processing steps, including the reduction of noise by data filtering, TWSA data from GRACE/-FO show spatially smoothed patterns. To make the WSCs compatible with TWSA for the subtraction process in terms of their spatial structure, GRACE-like filtering of the WSC data sets has been implemented, with a spatial Gaussian filter of which the filter strength has been specified through the analysis of the spatial autocorrelation characteristics of the storage data sets (Sect. 2.3.3). The re-sampled and filtered data sets are then subtracted from TWSA in a straight-forward algebraic operation (Sect. 2.3.4). The G3P processing chain also includes uncertainty propagation from individual uncertainty estimates of TWSA and each WSC into a total uncertainty estimate of the final GWSA data (Sect. 2.3.5).

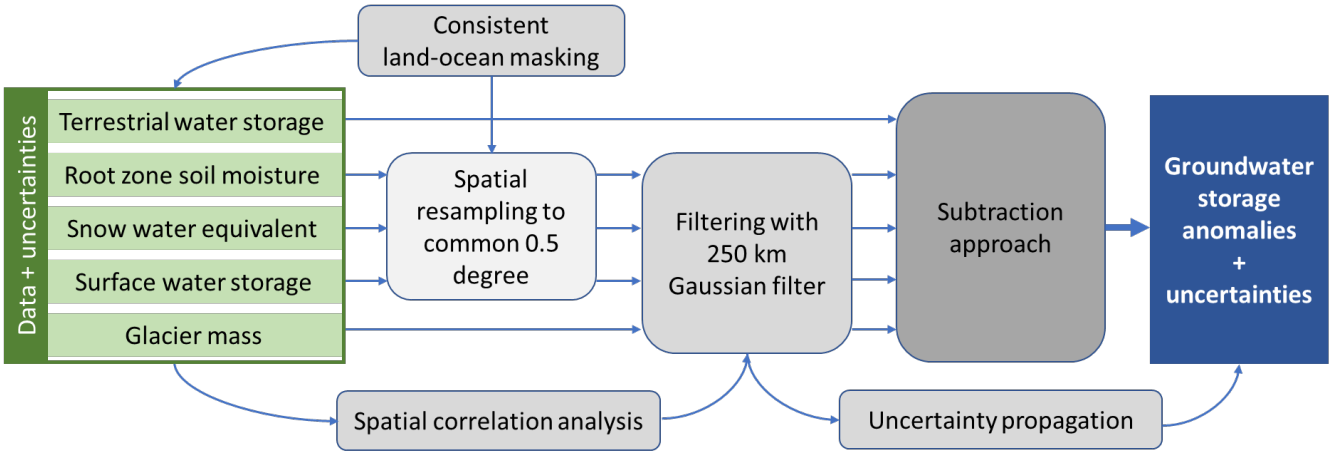

Figure 1: The G3P processing chain. All input data sets depicted in the green boxes are provided as monthly water storage anomalies relative to a long-term mean value.

2.2 Data

The data sets that serve as input for the G3P processing chain and the primary output data set are summarized in Table 1. TWSA is based on a combination product of different GRACE/-FO processing centres (Sect. 2.2.1). RZSM, SWE and GM are based on existing operational open-access data products of the Copernicus Climate Change Service and the Copernicus Land Monitoring Service, and further adapted to the needs for G3P generation (Sect. 2.2.2, 2.2.3, 2.2.4). SWS is based on the operational OS LISFLOOD hydrological model used for flood forecasting applications in the Copernicus Emergency Management Service (Sect. 2.2.5). The target data set GWSA finally is a combination product of the five aforementioned data sets, providing monthly groundwater storage anomalies with 0.5° nominal spatial grid resolution globally for all continental areas except Antarctica and Greenland. In its current version G3P V1.12 (Güntner et al., 2024), the GWSA data set covers the period 04/2002 to 09/2023. The anomalies are given relative to an arbitrary long-term mean, here calculated over the period 04/2002 – 12/2020, corresponding to the to the GRACE/-FO level 2B anomaly data (see chapter 2.2.1).

Table 1: The global WSC data sets of the G3P processing chain, with their source of acquisition, spatial and temporal resolution and coverage, and the data services from which the data sets are further adapted for G3P integration as described in this paper. GWSA G3P V1.12 is the target data set provided in this paper. Abbreviations: in situ observations (G); satellite observations (S); reanalysis (R); hydrological models (M); Combination Service for Time-variable Gravity Field (COST-G); Copernicus Climate Change Service (C3S); European Space Agency Climate Change Initiative (ESA-CCI); Copernicus Land Monitoring Service (CLMS); Copernicus Emergency Management Service (CEMS)**.**

Data set name	Water storage	Data source	Spatial resolution	Temporal resolution	Temporal coverage	Data service
TWSA	Terrestrial water storage	S	0.5°	monthly	2002-2023	COST-G

RZSM	Root zone soil moisture	S	0.25°	daily	2000-2023	C3S
SWE	Snow water equivalent	S, R	0.05°	daily	2000-2023	CLMS
GM	Glacier mass	S, G	0.5°	monthly	2000-2023	C3S
SWS	Surface water storage	M	0.05°	daily	1970-2023	CEMS
GWSA	Groundwater storage	S/G/R/M	0.5°	monthly	04/2002-09/2023	G3P V1.12

2.2.1 Terrestrial water storage anomaly (TWSA)

The TWSA data set (a Level-3 product) is derived from temporal variations of the gravity field of the Earth, initially represented by a series of spherical harmonic (SH) functions and the corresponding sets of SH coefficients (called Stokes coefficients; a Level-2 product) (Tapley, 1989). The GRACE/-FO satellites provide gravity information by acting as test masses in a free fall experiment. The gravitational acceleration acting on the satellites is computed by the so-called "dynamic approach" (Tapley, 1989) from the satellites' trajectories, determined by GPS observations, and from the change in inter-satellite distance, observed with micrometre accuracy via a K-band microwave link (Tapley et al., 2004) or with nanometre accuracy using a Laser Ranging Interferometer technology demonstration on GRACE-FO (Abich et al., 2019). A near polar orbit with an inclination of 89.5° of the satellite pairs enables the computation of a global gravity field of the Earth. After one month, a spatial resolution of the gravity field of 200 - 300 km is achieved, depending on latitude and the actual orbit constellation during the particular month (Flechtner et al., 2016). To isolate the hydrological gravity variations of interest, mass change signals of oceanic, atmospheric, terrestrial and polar tides are removed. Non-tidal mass variations of the ocean and the atmosphere on sub-monthly time scales are reduced by the so-called atmosphere and ocean de-aliasing Level-1B (AOD1B, Dobslaw et al. (2017) products based on ECMWF atmospheric analysis data and an ocean circulation model (Shihora et al., 2022). The remaining temporal variations of the monthly gravity fields mainly encompass hydrological mass variations of water in liquid and solid form, and geodynamic variations of the Earth's crust, i.e., global isostatic adjustment and co-seismic deformation. GRACE/-FO processing towards the gridded TWSA product can be split into three parts as further described in the following: (i) processing of Stokes coefficients (Level-2); (ii) corrections to the Level-2 data in the SH domain (Level-2B); and (iii) SH synthesis to a gridded TWSA data set and corrections applied to the grids (Level-3).

Level-2 Processing

Due to the diverse observation types of the GRACE/-FO satellites and poorly known instrument noise characteristics, the inversion from the instrument data to a global gravity field, including different types of empirical and pseudo-stochastic parameters, is a complex process. Therefore, in combination with several gravitational background models that all have specific error budgets, the formal uncertainties of the SH coefficients of the monthly gravity fields are somewhat different among GRACE/-FO analysis centres (ACs) and only realistic when calibrated by empirical covariance modelling techniques (Lasser,

2023). In order to profit from the strengths of the different processing approaches and to reduce the stochastic noise in the individual monthly gravity field models, a combination of the solutions from different ACs is performed by the Combination Service for Time-variable Gravity fields (COST-G) (Jäggi et al., 2023). For G3P, the combination scheme, initially designed by the European Gravity Field Service for Improved Emergency Management (EGSIEM) (Jäggi et al., 2019), has been further developed and adapted for the combination of GRACE-FO gravity fields. Meyer et al. (2023) provide details on the GRACE-FO quality control and combination process. The resulting COST-G Level-2 combination product by the University of Bern is the basis for the TWSA data set used in G3P.

Level-2B Processing

During Level-2B processing, several corrections are applied to the Level-2 gravity field data, as detailed in Dahle et al. (2025) and summarized here. First, a mean field is reduced from all months to obtain gravity anomalies relative to the same epoch. Essentially, the choice of the long-term mean is arbitrary and has been defined for the current G3P version V1.12 and earlier versions to cover the period April 2002 - December 2020. We then filter the Stokes coefficients with the anisotropic VDK2, VDK3, and VDK5 filters (Horvath et al., 2018). This filtering is necessary to optimally separate signal from noise in the GRACE/-FO data. The number of the filter name indicates the filter strength, with VDK2 the strongest filtering used in the processing and VDK5 the weakest. Different filter strengths are necessary to obtain the optimal results by combining differently filtered gravity fields, see also Level-3 processing below.

The Stokes coefficient with degree 2 and order 0 (C20) is related to the flattening of the Earth and poorly observed by GRACE/-FO. Thus, this coefficient is replaced by an estimate derived from a combination of GRACE/-FO with satellite laser ranging (SLR). Further, the Stokes coefficient with degree 3 and order 0 (C30) is poorly determined by GRACE/-FO in periods when accelerometer observations for one of the two spacecraft are not available (as for GRACE from November 2016 till the end of the science mission phase in June 2017) or are degraded (as for the whole GRACE-FO mission). In these periods, available accelerometer observations of one satellite are transplanted to the other. By incorporating an improved accelerometer transplant product for GRACE-FO (Behzadpour et al., 2021), the C30 coefficient is well determined and thus does not need to be replaced anymore for GRACE-FO. For the last seven months of the GRACE mission, C30 is replaced with estimates obtained from the same GRACE/-FO and SLR combination as mentioned above for C20. The GRACE/-FO observations system is insensitive to geocentre motion, which is related to the Stokes coefficients of degree 1 (C10, C11, and S11). Thus, these coefficients are set to zero by definition in the Level-2 data. In order to correctly estimate the terrestrial mass distribution, we approximate these coefficients using the approach described in Swenson et al. (2008) and insert them into the Level-2B products.

The Earth's gravity field is affected by long-term secular trends due to Glacial Isostatic Adjustment (GIA), mainly in previously glaciated regions such as North America, Fennoscandia and Antarctica. The Level-2B products are corrected using the GIA model ICE-6G_D (VM5a) (Peltier et al., 2018). Finally, a harmonic signal at the frequency of 161 days, the alias frequency of the semi-diurnal solar tide S2, is fitted to the time series of Level-2 products and subtracted from the Level-2B products.

Level-3 Processing

The Level-3 processing (see Dahle et al. (2025) for details) primarily uses Level-2B data filtered with VDK3 and VDK5. VDK2 is only used for months with low data quality (explained below). The first step converts the Level-2B Stokes coefficients to a global 0.5° grid of monthly mass anomalies, expressed as equivalent water height. We decompose these gridded data into the linear trend, the annual and the semi-annual sinusoidal signals (estimated with least squares adjustment) and the residual inter-annual signal. In order to reduce the influence of leakage, the deterministic signals (trend, annual, semi-annual) are taken from the fields that have been filtered with the weaker VDK5 filter and are combined with the stronger filtered VDK3 residual signal. For each month, we compare the global standard deviation of the residuals over the open ocean (distance to coast > 1000 km) to the mean of these standard deviations averaged over all months. If the standard deviation of a given month is twice as large as the mean standard deviation, we use the residuals from the even stronger filtered VDK2 field. For the available GRACE/-FO data set from 2002 to 2023, only February 2015 of the GRACE mission is affected by this stronger filtering.

Level-3 processing finally includes the removal of mass changes due to co-seismic deformations caused by the megathrust earthquakes of Sumatra-Andaman (2004), Chile (2010), and Japan (2011). This is done by estimating a step function in a spherical cap with a radius of 1000 km around the epicentre. The resulting data set represents the monthly TWSA data used in the subsequent G3P processing chain towards generating the groundwater product. Uncertainties of the TWSA data are provided as a grid-scale standard deviation, computed as the root mean square error (RMSE) of the residual signal over the open ocean (distance to coast > 1000 km) scaled by a spatial covariance model (Boergens et al., 2022; Boergens et al., 2020).

2.2.2 Root-zone Soil Moisture (RZSM)

Root-zone soil moisture is the water present in the soil column where plant roots directly access water and nutrients. Practically, and in most models, it is defined as the water stored in the upper 1 to 2 meters of soil (Hirschi et al., 2014; Mishra et al., 2020), although the actual rooting depth may vary, e.g., as a result of plant species, geology, and climatic conditions (Fan et al., 2017). Especially in water-limited regions, RZSM controls plant growth and photosynthesis, plant water stress, and crop yield (Martens et al., 2017; Vreugdenhil et al., 2022).

The root-zone soil moisture product used in G3P is a long-term (2002-2023), global, gap-free data record based on the multi-satellite surface soil moisture (SSM) climate data record provided by the Copernicus Climate Change Service (Dorigo et al., 2018). Direct measurements of RZSM are only available at few, unevenly distributed in situ stations (Dorigo et al., 2021a). On the other hand, microwave satellite observations, such as the ones integrated in C3S SSM are globally available but only sensitive to water in the topsoil layer (~ 5 cm) (Gruber et al., 2019). The RZSM product used by G3P seeks to make optimal use of both, without the intervention of any land surface of hydrological modelling (Pasik et al., 2023). To do so, it first fills gaps in the C3S SSM product related to, e.g., seasonal masking or instrument unavailability, to obtain global seamless coverage, and subsequently converts the gap-free SSM to RZSM using an infiltration model that has been calibrated with ground-based observations. Both methods are briefly summarised here.

Data gaps in the SSM product are filled using a standalone interpolation method (Preimesberger et al., 2025). This means that the gap-filling uses only available neighbourhood information (temporally and spatially) and that the resulting values are therefore independent of any other data records or ancillary data. The used method is based on the discrete cosine transform (DCT) penalized leased squares (PLS) method, which was initially designed as a smoothing algorithm (Garcia, 2010). The aim of the algorithm is to find a set of smoothed values $\hat{y}$ to represent the original input data y with (i) minimal Residual Sum of Square (RSS) and (ii) optimal reduced roughness $P(\hat{y})$ between (smoothed) elements as described in Eq. (2). Missing values are interpolated as part of the smoothing process and finally used to fill gaps in the observational data.

$$F(\hat{y}) = RSS + P(\hat{y}) = \|y - \hat{y}\| + s\,P(\hat{y}) \tag{2}$$

The parameter s in Eq. (2) is the only free model parameter that is optimised using a generalised cross validation (GCV) approach described in Eq. (3).

$$GCV(s) = \frac{wRSS/(n-n_{miss})}{(1-Tr(H)/n)^2} \tag{3}$$

This iteratively optimises the interpolation function via weighted residuals ($wRSS$) with H being the hat matrix from the PLS controlling the trade-off between goodness of fit and smoothing between observations (n and n_{miss} refer to the number of available and interpolated data points).

This algorithm was already widely used to interpolate SSM, generally with good performance that is on par with other, more complex, and often covariate-dependent methods (e.g., Shangguan et al. (2023); Guo et al. (2022)). DCT-PLS is applied on a moving window basis, meaning the smoothing parameter s is locally tuned from data within a 15° bounding box, to take into account globally changing levels of soil moisture variability within different climate regimes. Soil moisture during seasonally

frozen periods (identified from modelled ERA5 soil temperature data (Hersbach et al., 2020) is linearly interpolated over time to represent a constant or slowly changing level of stored (frozen) water in the soil.

SSM is then converted to RZSM using an exponential filter (EF) based model (Pasik et al., 2023; Albergel et al., 2008) which simulates the drainage of water from the surface into deeper layers, by smoothing and delaying the measured SSM signal. Various studies have shown that this yields a good approximation of actual root-zone conditions, especially for layers until about 1 m depth (Paulik et al., 2014; Wang et al., 2017). Eq. (4) summarises the method:

$$RZSM(t_n) = RZSM(t_{n-1}) + K_n \cdot \left(SSM(t_n) - RZSM(t_{n-1})\right) \quad (4)$$

RZSM at time $t_{_n}$ is approximated by a weighted combination of the SSM observation made at $t_{_n}$ and preceding RZSM at $t_{_(n-1)}$. The gain factor K ranges from 0 to 1 and is calculated as follows (Eq. 5):

$$K_n = \frac{K_{n-1}}{K_{n-1} + e^{-\frac{t_n - t_{n-1}}{T}}} \quad (5)$$

At initialization, when no preceding estimates are available, the EF calculation is started with K_0=1 and RZSM(t_0)=SSM(t_0). However, the EF model is purely time-based, integrating weighted surface observations over a pre-defined preceding period (T). There is no parameter controlling the actual infiltration depth. Hence, to allocate T to depth layers, Pasik et al. (2023) optimised EF based RZSM with measured in situ RZSM to find T-values (6, 15, 48, 70) that best represent RZSM at the four corresponding depth layers (0-10, 10-40, 40-100, 100-200 cm) globally. The optimised T-value for each depth layer is the one that maximises the Pearson correlation between satellite soil moisture, after applying the EF to the SSM estimates, and field measurements taken within that depth interval, sourced from the International Soil Moisture Network (ISMN).

Uncertainties in the satellite SSM observations are estimated using Triple Collocation Analysis (TCA) (Gruber et al., 2016). They represent spatially varying levels of (random) error variance ("noise") for each of the merged sensors relative to the strength of the retrieved soil moisture signal. This depends on the sensor characteristics such as the observation frequency band, in conjunction with confounders such as vegetation density. Uncertainties from the SSM product are propagated through the EF to subsequently describe RZSM uncertainties (De Santis and Biondi, 2018). To account for the considerable uncertainty the EF introduces when approximating RZSM from surface observations, Pasik et al. (2023) introduced an additional term to the error propagation, i.e. the model structural error $\sigma^2(EF)$. This uncertainty component was quantified using in situ observations from stations measuring SSM as well as RZSM. For these stations, the EF is applied to in situ SSM to simulate in situ RZSM. The discrepancy between the predicted and observed RZSM represents $\sigma^2(EF)$ for the respective integration depth. $\sigma^2(EF)$ was found to increase with depth ranging from 0.03 m^3m^{-3} at layer 1 to 0.04 m^3m^{-3}at layer 4.

The RZSM data is influenced by uncertainties in input SSM measurements, as well as the assumptions made during gap-filling and the conversion from SSM to RZSM, as described above. The quality of the generated RZSM data varies temporally and spatially due to the coverage of available satellite observations and the uneven global distribution of in situ stations.

2.2.3 Snow Water Equivalent (SWE)

The water content of a snow cover is described by the ECV quantity SWE. Satellite remote sensing with passive microwave sensors (PMR) allows for spatially and temporally continuous SWE monitoring. However, current satellite remote sensing-based SWE products are available for the Northern hemisphere only (Pulliainen et al., 2020). To cover the full globe and the GRACE/-FO period from 2002-2023 as required for G3P processing, a combined SWE product derived from PMR satellite observations and model-based SWE from MERRA2 an ERA5-Land was developed here. Satellite-based SWE for the period of 2002-2005 is derived from GlobSnow v3.0 (https://www.globsnow.info/), while the Copernicus Land Monitoring Service (CLMS) SWE product (https://land.copernicus.eu/global/products/swe) serves as baseline input for the years 2005-2023. GlobSnow v3.0 SWE is available on a 25 km EASE grid, CLMS SWE produced in Near-Real-Time (NRT) is available on a 0.05 x 0.05° geographical latitude/longitude grid. Both satellite SWE datasets apply the retrieval methodology by Luojus et al. (2021). The SWE retrieval combines PMR measurements with ground-based synoptic weather station observations via Bayesian non-linear iterative assimilation. The GlobSnow v3.0 SWE includes monthly bias-correction (Pulliainen et al., 2020) which significantly enhances the retrieval results. A detailed description of the PMR-based SWE methodology is given in Luojus et al. (2021).

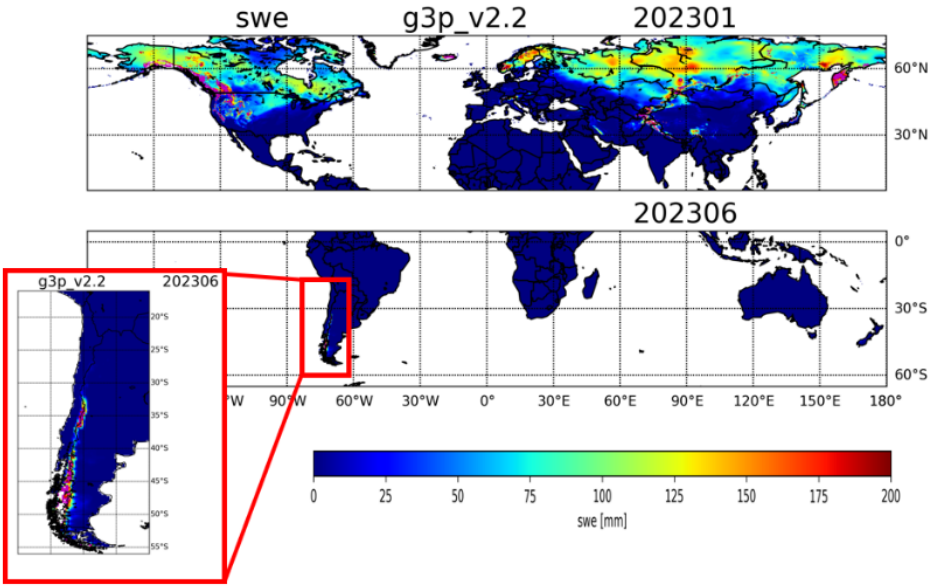

Figure 2: Example of the snow water equivalent SWE data set with global coverage from the G3P combined satellite and model product v2.0 for the months of June 2023 (southern hemisphere) and February 2023 (northern hemisphere).

The Southern Hemisphere remains a challenging area in remote sensing of SWE with PMR. Additionally, mountain areas are not covered in the standard GlobSnow and CLMS operational SWE products. To fill these gaps, a merged product using SWE from satellites and models has been established (Fig. 2). Simulated SWE from three land surface models and reanalysis systems was examined: GLDAS2.2 LIS (Li et al., 2019), ERA5-Land (Muñoz-Sabater et al., 2021) and MERRA2 (Gelaro et al., 2017). The skilfulness of the all datasets was evaluated by comparing to in situ SWE observations from snow course transect measurements conducted across Russia (Bulygina et al., 2011), Finland (Haberkorn, 2019) and Canada (Brown et al., 2019). The in situ data consist of manual gravimetric snow measurements carried out at multiple locations along a pre-defined transect, of which an averaged value was used as representative for the corresponding pixel or grid cell of the model or remote sensing dataset to be validated. ERA5-Land and MERRA-2 resulted in the best validation results (Fig. 3, middle panel) while GLDAS2.2 showed a clear underestimation of SWE, especially in Canada, and was discarded for further processing. With a relatively high Spearman correlation of over 0.6 against the in situ observations throughout all years, both satellite baseline SWE products GlobSnow v3.0 as well as CLMS SWE perform well in the Northern hemisphere (Fig. 3, left panel). All satellite- and model-based datasets were resampled with bilinear interpolation to a common resolution on a regular 0.25° grid to allow for merging. The gaps of the satellite-based data were then filled with the grid-cell mean SWE value of ERA5-Land and MERRA-2 to achieve full global coverage, excluding the area covered by glaciers ((Rgi, 2017); Sect. 2.2.4). The validation results of the final merged G3P SWE product version v2.0 with respect to in situ observations is shown in Fig. 3, right panel.

Overall, the validation results such as the site-specific and averaged correlation coefficients showed reasonable performance of the estimated SWE values, especially for winter months with high absolute snow mass.

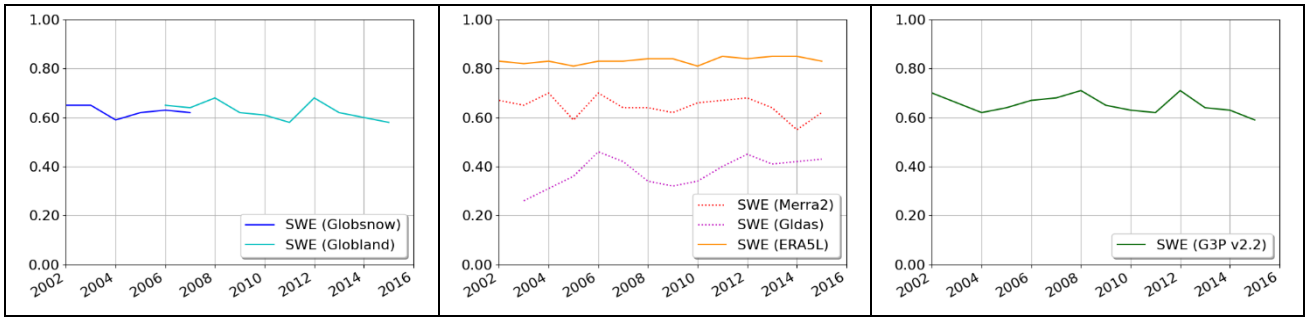

Figure 3: Mean annual Spearman correlation coefficient between SWE products and in situ snow course measurements distributed over Northern hemisphere in Russia, Canada and Finland; left: satellite products GlobSnow 3.0 and CLMS; middle: model products MERRA-2, GLDAS2.2 and ERA5-Land; right: G3P SWE product version v2.0

The satellite-based SWE data of GlobSnow and CLMS offer pixel-scale uncertainties which were derived by error propagation from raw satellite data through the algorithm, see Takala et al. (2011) and (Pulliainen, 2006) for details. The reanalysis models used for gap filling do not provide SWE uncertainties, though. In this case, grid-scale uncertainties were obtained by diagnostic uncertainty estimates as the absolute difference between the model-based and the in situ-based SWE. A summary of existing prognostic and diagnostic approaches for quantifying uncertainty and evaluating uncertainties is given in Sayer et al. (2020).

2.2.4 Glacier Mass (GM)

The glacier mass change product for the G3P processing chain builds on the combination of input data and auxiliary data brokered from international data repositories. As input data, we use the glacier mass change global gridded data available from the C3S Climate Data Store (CDS) (Dussaillant et al., 2023). This dataset is based on glaciological and geodetic time series of glacier mass and elevation changes, respectively, as available from the Fluctuation of glaciers database (FoG) brokered by the World Glacier Monitoring Service WGMS (Wgms, 2023). As auxiliary dataset, we use the glacier distribution data also available from the C3S CDS (Cdr, 2024). In turn, this dataset is based on the Randolph Glacier Inventory RGI 6.0 (Rgi, 2017), which is a community product generated within the RGI working group of the International Association of Cryospheric Sciences (IACS). For more details on these input and auxiliary datasets, we refer the reader to the C3S related product documentation.

For G3P, inspired by previous methodological frameworks (Zemp et al., 2020; Zemp et al., 2019), we developed a new approach to combine the temporal variability of the glaciological in situ observations with the long-term change rates of

geodetic observations - mainly from satellites - for all glaciers existing in the RGI inventory (Dussaillant et al., 2025). For the G3P processing chain, all individual WSCs need to deliver their data sets with monthly temporal resolution. This was a major challenge for the glacier compartment, since glacier observations are available only in multi-annual, annual, or at most, seasonal temporal resolutions. Still, accurate globally integrated glacier changes can only be achieved at a minimum annual temporal resolution. For G3P we further developed our methodology to obtain distributed glacier changes at monthly temporal resolution by applying a seasonal sine wave function, informed by the available winter and summer mass change observations Zemp and Welty (2023) over the annual glacier changes from Dussaillant et al. (2025). The down-sampling of annual glacier observations to monthly resolution comprise large assumptions which are reflected in the large uncertainties of the glacier change product used in G3P.

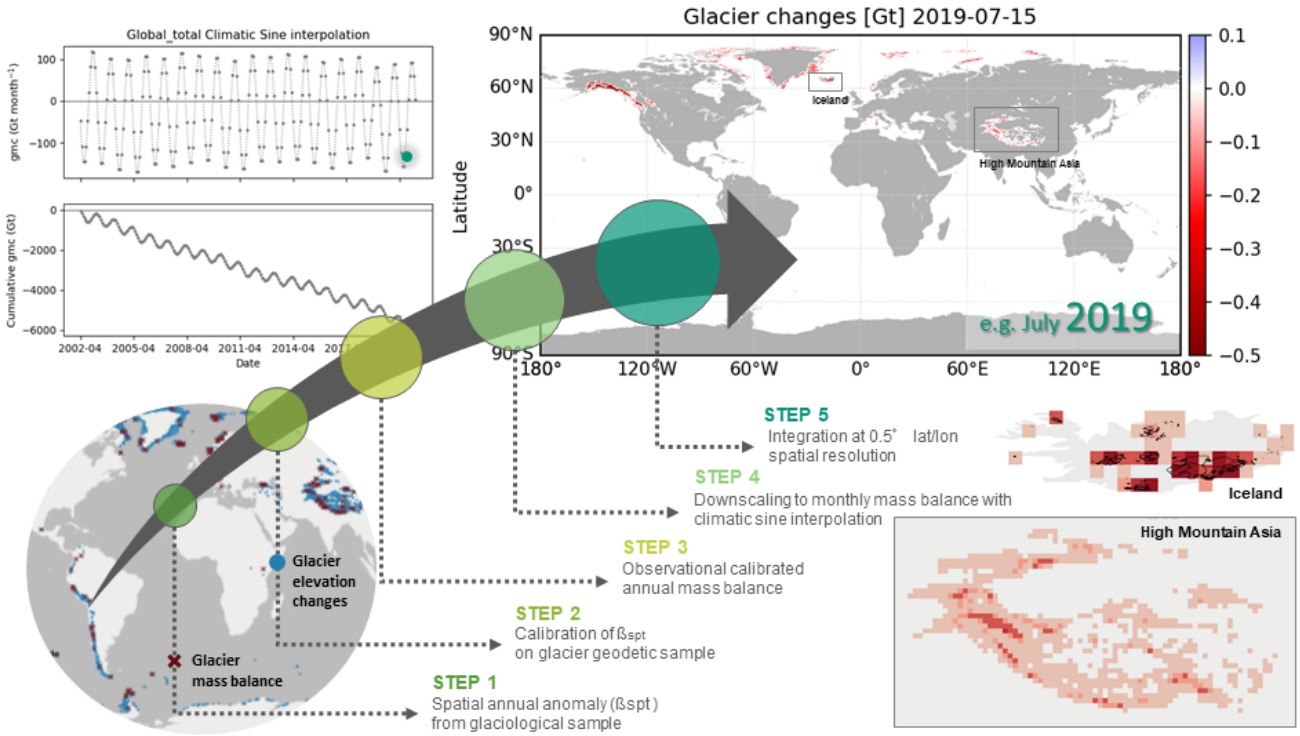

Figure 4: Summary illustration of the five main processing steps to produce global monthly glacier mass changes for the GRACE/-FO period (April 2002 to September 2023) spatially distributed in a global regular grid

Our algorithm produces a global gridded product of monthly glacier changes in five processing steps summarized in Fig. 4. First, for each glacier of the RGI 6.0, we estimate the detrended temporal variability of annual mass change of the glacier (calculated as the glacier mean annual mass change anomaly with respect to the reference period 2011-2020) using the interannual variability of nearby glaciological time series. Second, we calibrate the mean annual mass balance anomaly to all

available long-term trends from the geodetic samples available for the respective glacier. Third, we integrate all of these calibrated time series into a single weighted average, considering the uncertainty as well as the temporal coverage of the geodetic surveys. This results in a data-fused mean calibrated annual mass change time series that is unique for every individual glacier. Fourth, for every region, we build a regional seasonal sine curve from all available seasonal (winter and summer) mass balance observations of this region. Years without seasonal observation are fitted on a climatic mean winter and summer value calculated per region. We then interpolate the regional sine wave over each individual glacier, by fitting the individual annual values from the mean calibrated annual mass change time series from step 3. The mean calibrated monthly mass change time series are interpolated for each region following the hydrological year monthly distribution (1st October to 30th September in the Northern Hemisphere; 1st April to 31th March in the Southern Hemisphere), except for glaciers in low latitude regions where we linearly interpolate through the year due to the lack of winter and summer seasons. Finally, we aggregate the mean calibrated monthly mass change time series as an area-weighted mean in a global regular grid of 0.5° to fit the G3P resolution.

The glacier product uncertainty estimation for annual values is described in detail on the C3S glacier mass change global gridded product documentation (see above). When applying the regional seasonal sine curve to downscale to monthly data (Step 4), the mean annual mass change time series uncertainty is multiplied by 1.5 to get the relative monthly uncertainty. This multiplication factor is somewhat arbitrary, but it ensures that the monthly downscaled product has a larger uncertainty than the annual product. A thorough accuracy assessment and validation is also available for the C3S annual glacier mass change global gridded input dataset by (i) comparing the annual estimates with previous global studies from annual direct observations (Zemp et al., 2019; Hugonnet et al., 2021) and by (ii) performing a detailed leave-one-block-out cross-validation experiment of mean calibrated annual mass change estimates over selected reference and benchmark glaciers. The accuracy of the downscaled monthly glacier changes was analysed by comparing with monthly glacier changes derived from GRACE (e.g., Wouters et al. (2019). There is a good agreement at the global level but the amplitude of the seasonal cycle of our glacier mass change is smaller than the one derived from GRACE. We note that our uncertainty assessment is still rather on the first order, further developments are still needed to propagate annual uncertainties to monthly estimates and to validate the accuracy of the seasonal cycle of our glacier mass change product at monthly time resolution (an effort currently accounted by the international community through the GlaMBIE project; https://glambie.org).

Our final product provides monthly glacier mass changes (in Gigatonnes per year) and related uncertainty at global scale with a spatial resolution of 0.5° for the entire GRACE/-FO study period. Yearly updates based on the integration of latest glaciological balances from the FoG database are possible with a lag of one year. The basic concept of the approach, latest improvements of the methodology, and a detailed leave-one/block-out cross-validation is given in Dussaillant et al. (2025) and is ready for implementation in future versions of the G3P product.

2.2.5 Surface Water Storage (SWS)

SWS includes water stored in rivers, lakes, man-made reservoirs and wetlands. Several promising approaches have been explored in the past years to quantify these components, some of which have also been tested in the context of G3P development: For estimating river storage, the semi-operational hydrological forecasting platform HYFAA which couples the MGB model (Collischonn et al., 2007) with data assimilation of water level data from satellite altimetry was set up for the Niger and Congo basin, with positive validation results when compared to in situ discharge data and global hydrological models. For a set of 250 lakes operationally monitored in the Copernicus Global Land Service and an additional 150 lakes from different sources, lake storage time series were calculated using satellite altimetry and hypsometric curves linking lake water level and extent (Crétaux et al., 2018). However, neither approach results in the required global coverage for G3P. Further promising efforts include the DAHITI project (Schwatke et al., 2015), offering satellite-altimetry-based lake level time series for over 10,000 lakes or the Satellite-based Wetland Observation Service (SWOS) (Weise et al., 2020). At the time of developing G3P, however, there was no observation-based surface water storage product with global coverage available, less so for a holistic assessment of all the surface water components, i.e., rivers, lakes and man-made reservoirs.

For this reason, the SWS data for the G3P version presented here are not observation-based but derived from the global hydrological model OS LISFLOOD (Van Der Knijff et al., 2010) in its implementation in the Copernicus Emergency Management Systems' Global Flood Awareness System (GloFAS) version 4.0 (Choulga et al., 2024), complemented with observations for the Caspian Sea from the DAHITI project (Schwatke et al., 2015) as this lake is not considered in OS LISFLOOD. OS LISFLOOD output has a daily resolution on a 0.05° grid (3 arcmin). From the model output, we derived global-scale river storage and storage in 463 lakes and 687 reservoirs worldwide, with varying degrees of further processing as described below. Depression storage and interception storage were not considered in the G3P surface water product due to their negligible storage variations. While OS LISFLOOD in the version used here does not explicitly represent wetland dynamics, inundated areas are considered by widenings of the channel profile.

As a first processing step, all relevant OS LISFLOOD output files were aggregated from daily to monthly values and resampled from the native 0.05° to the common 0.5° G3P grid. OS LISFLOOD river storage was calculated by multiplying the river length per grid cell given as model input with the state variable of channel cross-sectional area of water flow, which is available for each grid cell as mean value per model time step.

For calculating lake and reservoir storage variations, three major issues need to be resolved: (i) OS LISFLOOD depicts a lake or reservoir as part of the river network, represented in the model by a single grid cell at the location of the outlet of the waterbody, even if its area exceeds the size of this cell. For the purposes of G3P, where a spatially accurate water mass distribution is required, the water stored in this one cell has to be re-distributed to the real-world spatial extent of the lake. (ii)

The river water storage of the cells that fall into the area of a lake or reservoir has to be added to the storage of that waterbody. (iii) Reservoir storage can simply be calculated by multiplying the model input layer of reservoir storage capacity, given as a volume in m³, with the simulated time-variable state of reservoir filling, given as a percentage value in the model output. The OS LISFLOOD lake routine, however, only calculates lake water level variations but not the volume changes.

Thus, the routine for calculating lake and reservoir storage for G3P includes the following steps: (i) for each outlet cell of a waterbody, the corresponding lake or reservoir polygon was selected from the Global Lake and Wetland Database (GLWD) (Lehner and Döll, 2004). In case of an ambiguity, we checked if one of the conflicting waterbodies already had another outlet cell, otherwise we chose the larger one; (ii) all 0.5° grid cells of which the centre point is inside the polygon were assigned to the waterbody. This ensures that every grid cell can only be part of one lake or reservoir; (iii) lake or reservoir volume variations were computed from OS LISFLOOD output by multiplying the simulated water level at each time step with the lake area from GLWD; (iv) the resulting water volume was distributed over all grid cells assigned to the lake or reservoir, (v) river storage of each grid cell that was assigned to the lake or reservoir was summed up and evenly distributed over the area of the waterbody and added to its storage; (vi) cells assigned to lakes or reservoirs were masked out of the river storage layer to prevent double accounting.

Finally, all surface water storage compartments (rivers, reservoirs and lakes) were converted to mm equivalent water height and combined to a single global data set of SWS anomalies. As OS LISFLOOD does not provide uncertainty estimates for its simulation results, a first-order SWS uncertainty assessment was used by calculating the SWS difference at each monthly time step and for each grid cell to the SWS simulation results of other global hydrological models, here the WaterGAP Global Hydrological Model (WGHM) (Schmied et al., 2021). The uncertainty value was then taken as half of this difference. This step was done after GRACE-like spatial filtering of both model-based SWS data sets (see Sec. 2.3.3) to mitigate errors that are only due to a subtle misalignment of surface water bodies in both models, e.g., if the location of a river stretch varies by one cell from one model to the other.

2.3 G3P processing

The G3P processing steps from the individual storage data sets described in the previous sections to the data sets of groundwater storage anomalies following Fig. 1 are detailed in the following sections.

2.3.1 Provision of consistent land-ocean masks

For a consistent combination of the individual WSCs and TWSA in the G3P subtraction process, it is important to assure that the water storage (water mass) information of all data sets is assigned to identical spatial units across the global, i.e., cells of a

global grid, both with respect to their geographic position and size, and also with respect to consistently assigning land and ocean areas across all data sets. As the basis for defining the land-ocean masks in G3P, we used the ESA CCI Water Bodies Map v4.0 (Lamarche et al., 2017) at 150 m resolution. This high-resolution map was aggregated to generate global land-ocean masks for each resolution at which the individual WSC datasets are produced. For the aggregation, the fraction of land f_{land} was calculated for each grid cell at the coarser resolution by considering the number of land pixels (nL) and ocean pixels (nO) of the high-resolution 150 m map according to Eq. 6:

$$f_{land} = \frac{n_L}{n_L + n_O} \tag{6}$$

For the target masks, all grid cells with $f_{land} > 0$ are classified as land cells, all other cells are classified as ocean cells. The target land-ocean mask with the binary land-ocean assignment at the required spatial resolution was then forwarded to each processing group of individual WSCs and of TWS, with the requirement of generating storage data for each land cell. The target masks deliver a large number of land cells globally, even though their actual land fraction can be very low. Nevertheless, this procedure guarantees that each individual storage data set is provided with uttermost spatial coverage at the global scale, preventing gaps in single data sets that would be adverse for the consistent data combination step later on.

It should be noted that at the 0.5° resolution, a second land-ocean mask was produced in which only the grid cells with $f_{land} > 0.5$ were classified as land cells. This land-ocean mask (output mask) was used to subset the 0.5° grid cells at the global scale for which valid storage data are provided after spatial filtering (Sect. 2.3.3) and in the G3P output files, excluding predominantly ocean-covered cells. The land-ocean masks are open-access available (see Sec. 5).

2.3.2 Data conversions and resampling

First, the individual WSC data sets with daily resolution were aggregated to a monthly resolution by taking the temporal mean for each month.

Second, the individual WSC and the TWSA data sets were, if needed, converted from their original units (such as mass in Gigatons) to the common unit of millimetre water equivalent (mm weq). This is done for each grid cell by dividing mass by the latitude-dependent grid cell area. For coastal cells (i.e., cells where $f_{land} < 1$, see Eq. 5), the storage value in mm weq is additionally multiplied by f_{land} in order to take into consideration that the storage value represents the land part of the cell only, being smaller than the total cell area.

Third, the cell-based time series of absolute monthly storage values of each WSC were transformed into anomaly time series (*WSCA*), representing the storage deviation at month *t* from an arbitrary time series mean value $\overline{WSC}$ (Eq. 7). This step is required as TWS data from GRACE/-FO cannot be given as absolute values of water storage, but only by monthly anomalies relative to a mean value, i.e., TWSA (or as TWS change from one month to another, not used here). For the data sets presented here, the period 04/2002 – 12/2020 was defined for calculating the time series means.

$$WSCA_t = WSC_t - \overline{WSC} \tag{7}$$

Fourth, the WSC data sets that were produced at a higher resolution than 0.5° (see Table 1) were resampled to this common target resolution using bilinear interpolation, as used in previous GRACE–hydrology studies (e.g., Ali et al. (2022)).

2.3.3 Spatial data filtering

Due to the nature of data acquisition and processing of GRACE/-FO and the need to reduce noise components, such as North-South-oriented stripes, gravity-based TWSA exhibit spatially smoothed patterns. Real-world water storage anomalies that are concentrated in comparatively small regions, such as surface water storage variations along a large river, for instance, will be represented in the TWSA data set smeared out over a few hundred kilometres. These spatial characteristics of gravity-based TWSA are reflected by high spatial autocorrelation values over large distances (Fig. 5).

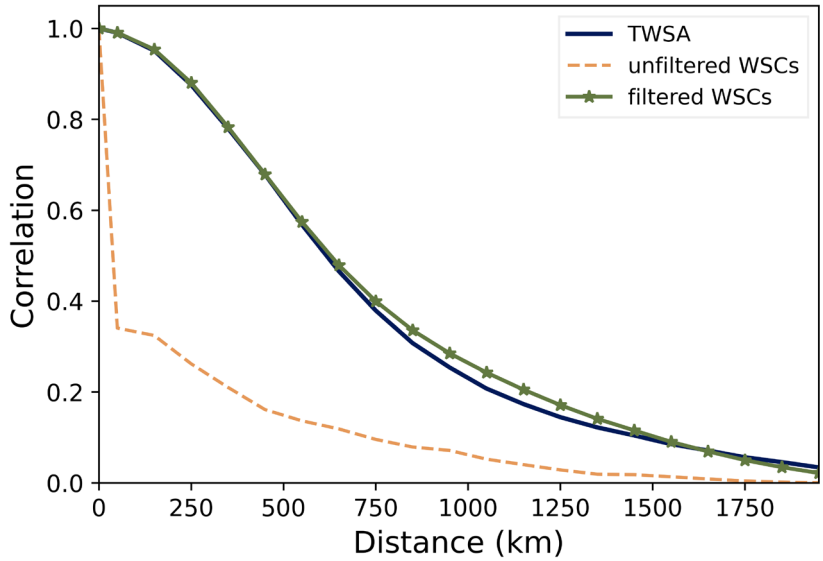

Figure 5: Globally-averaged empirical spatial autocorrelation functions of (i) GRACE/-FO-based TWSA, (ii) the sum of the four WSCs (RZSM, SWE, GM, SWS) and (iii) the sum of the four WSCs (RZSM, SWE, GM, SWS) after filtering with a 250 km Gaussian filter.

For a consistent data combination approach, such as in G3P where WSC data sets are subtracted from TWSA, it is imperative to have a similar spatial structure of the involved storage data. Otherwise, for example, subtracting spatially confined (non-smoothed) SWS anomalies from the smoothed TWSA may result in spurious groundwater storage anomalies at the locations of the SWS anomalies. One option to tackle this issue is by applying cell-based or river basin-based scaling factors to the TWSA data to restore signals that may have been smoothed out by the data processing steps before (e.g., Landerer and Swenson (2012), Long et al. (2015)). This approach comes with a considerable uncertainty in determining the scaling factors. They are usually derived from the comparison of simulated TWSA from hydrological models before and after spatial smoothing that is deemed to mimic the smoothing imposed by GRACE data processing. For G3P, we follow a different approach in which the WSC anomalies are smoothed in a GRACE-equivalent way before they are subtracted from TWSA. Sharifi et al. (2025a) show that smoothing the WSC anomaly data with the anisotropic DDK or VDK filter that is used for GRACE Level-3 processing (see Chapter 2.2.1) leads to spurious striping features in the filtered WSC data. GRACE-equivalent filtering is thus achieved by optimizing the strength of an isotropic Gaussian spatial filter (Jekeli, 1981) in a way that the empirical spatial autocorrelation function of the filtered WSC data matches the observed spatial autocorrelation function of gravity-based TWSA to the best possible form. The approach is described in detail in Sharifi et al. (2025a), resulting in an optimal filter width of the Gaussian filter of 250 km (Fig. 5). Herein, the filter width represents the radius at which the spatial filter weighting function declines to 50 % of its maximum value. Sharifi et al. (2025a) furthermore show that filtering of the four WSC anomaly data sets (RZSM,

SWE, GM, SWS) individually and then building the sum of the four is equivalent to first computing the sum of the four WSCs and then applying the Gaussian filter. Given its lower computational effort, the second approach, i.e., filtering of the combined WSCs anomaly data, was taken in the G3P processing chain described here.

2.3.4 Subtraction

Following the basic approach of Eq. 1, the combined and filtered WSC anomalies (see Sect. 2.3.3) were subtracted from TWSA in a simple algebraic cell-based operation for each month with available GRACE/-FO data within the data set period 04/2002 to 09/2023. This step was performed for all 0.5° land cells as defined by the output land-ocean mask (see Sect. 2.3.1), and excluding Greenland and Antarctica.

2.3.5 Uncertainty estimation

The individual WSC data sets are provided with gridded monthly time-varying uncertainties denoted as σ. After converting these uncertainties into the unit mm weq (see Sec. 2.3.2), they underwent a Gaussian filtering process in a similar way as the storage anomalies data (Sect. 2.3.3). The uncertainty of the resulting groundwater storage anomaly data set was calculated by standard uncertainty propagation following Eq. 8 at the 0.5° grid cell scale.

$$\sigma_{GWSA} = \sqrt{{\sigma_{TWSA}}^2 + {\sigma_{RZSM}}^2 + {\sigma_{SWE}}^2 + {\sigma_{GM}}^2 + {\sigma_{SWS}}^2} \tag{8}$$

2.4 Evaluation with in situ groundwater observations

Three examples for evaluating the G3P groundwater storage anomalies against in situ groundwater observations are provided in this study. Three major aquifers across the world were selected for this analysis: the Paris Basin in France (Europe), the High Plains Aquifer in the United States (North America), and the Guarani Aquifer system in Brazil (South America) (Fig. 6). These aquifers are comparatively well monitored and represent a variety of hydrogeological settings and climatic conditions, making them suitable for in situ evaluation of G3P. Detailed descriptions of the aquifers are presented together with the evaluation results in Sect. 3.4.

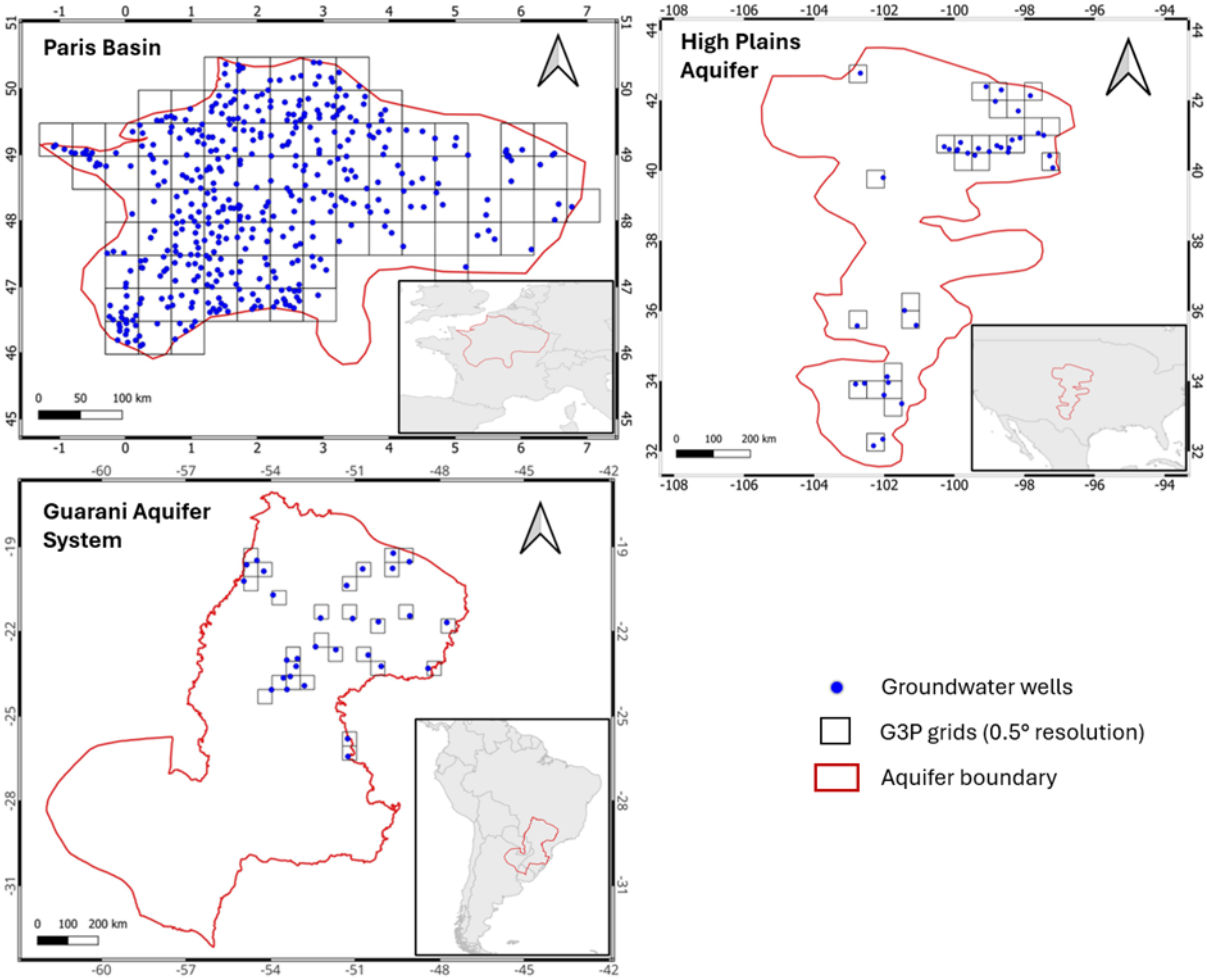

Figure 6: The three example aquifers for G3P evaluation against in situ groundwater data (Paris Basin, High Plains Aquifer, Guarani Aquifer) with the selected groundwater monitoring wells and the corresponding 0.5° grid cells from the G3P GWSA data set.

In situ groundwater level time series were obtained from the Global Groundwater Monitoring Network (GGMN) portal, which is a collaborative initiative operated by IGRAC that collects and shares groundwater monitoring data from national and sub-national authorities (Igrac, 2025). Specifically, Paris Basin data were contributed by the French Geological Survey (BRGM), High Plains Aquifer data by the United States Geological Survey (USGS) and Guarani Aquifer system data by the Geological Survey of Brazil (SGB). The raw datasets include 6070, 1872 and 95 boreholes for the Paris Basin, the High Plains Aquifer and the Guarani Aquifer system, respectively. The time series were processed to monthly resolution with outlier removal. To maximize in situ data inclusion and representativeness, relatively relaxed exclusion criteria were applied, i.e., allowing time series with up to of 20% missing data of the total record and gaps of up to 6 consecutive months within the study period from

April 2002 to September 2023. For the Guarani Aquifer system, data were available from October 2011 onwards only. Remaining data gaps were filled with a linear interpolation. Although the selected aquifers are already among the well monitored systems, these requirements still led to the exclusion of a substantial number of observation points. The final datasets include 440, 53 and 32 observation wells with monthly groundwater level time series for the Paris Basin, the High Plains Aquifer and the Guarani Aquifer system, respectively (Fig. 6). These data were converted into time series of groundwater level anomalies (GWLA) by removing a long-term mean level, similar to the computation of GWSA with GRACE/-FO data (see Sect. 2.3.2). To compute the aquifer-level GWLA, a grid-based averaging method was applied. The observation wells were assigned to the G3P grid cell in which they are located. Cell-level averages were computed in the case that more than one observation well is located within one G3P grid cell. The latter approach was used to mitigate spatial bias due to clustered boreholes. Then, GWLA time series of all relevant grid cells in an aquifer were averaged to obtain the aquifer-average time series.

The G3P GWSA data described in Sect. 2.3 were gap-filled for missing months with linear interpolation, except for the big gap from 2017 to 2018 between the GRACE and GRACE-FO satellite missions. For each of the three evaluation aquifers, aquifer-average GWSA time series and their uncertainties were computed by averaging across all G3P grid cells that contain in situ-based GWLA time series.

Finally, to make the GWSA and GWLA time series of each aquifer more comparable, both were standardized by removing the respective mean and by dividing with the standard deviation. Pearson correlation coefficients were calculated between the standardized GWLA and GWSA time series to assess the similarity of the observed groundwater dynamics.

3 Results

3.1 Examples of G3P groundwater storage dynamics

The seasonal amplitude of the GWSA is shown in Fig. 7. It is derived by, first, computing the mean seasonal dynamics of GWSA, i.e., its climatology, for each grid cell. For each month of the climatology, all available monthly GWSA values of this particular month throughout the data period are averaged. Then, the seasonal amplitude represents the difference between the maximum and the minimum GWSA among all 12 months of the climatology. The largest seasonal groundwater storage variations occur in the humid tropics of South America, followed by regions in South-East Asia with monsoon impact, and inner-tropical areas of Africa. While arid and temperate climates exhibit comparatively small seasonal GWSA amplitudes, intermediate values show up for several high-latitude regions in Eurasia and in North America.

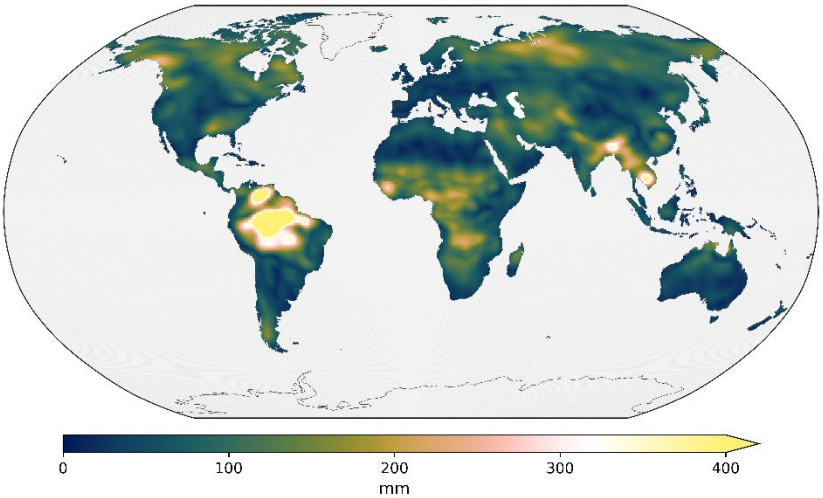

Figure 7: Seasonal amplitude of GWSA (average over the years 2002-2023)

The globally averaged climatologies of all WSCs and of TWSA are shown in Fig. 8. GWSA has the largest seasonal amplitude among all WSCs (i.e., excluding TWSA), followed by SWE. Temporal lags between the seasonality of WSCs are obvious, with SWE having its maximum in the northern hemisphere winter months, and SWS peaking in the period May to July. The global maximum of GWSA occurs in May and the minimum in October. As a consequence of the superposition of all individual WSC dynamics, the maximum TWSA on the continents occurs in April. For the months with maximum and minimum GWSA, the global distribution is shown in Fig. 9.

Figure 10 maps, the spatial distribution of the month in which the maximum GWSA occurs throughout the year in each grid cell. In temperate and Mediterranean climate zones, the maxima tend to occur towards the end of the winter months or in the spring months of the respective hemisphere, after the period of minimum evapotranspiration, and after snowmelt (where relevant) comes to an end. In tropical areas maxima are often related to the occurrence of the rainy season such as the Monsoon period in south-eastern Asia.

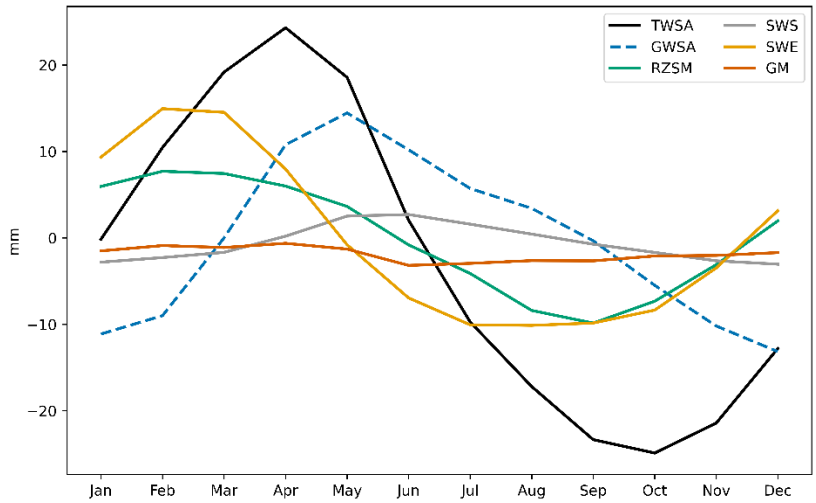

Figure 8: Globally averaged seasonal storage variations (climatology) of the different water storage compartments and of TWSA (period 2002-2023)

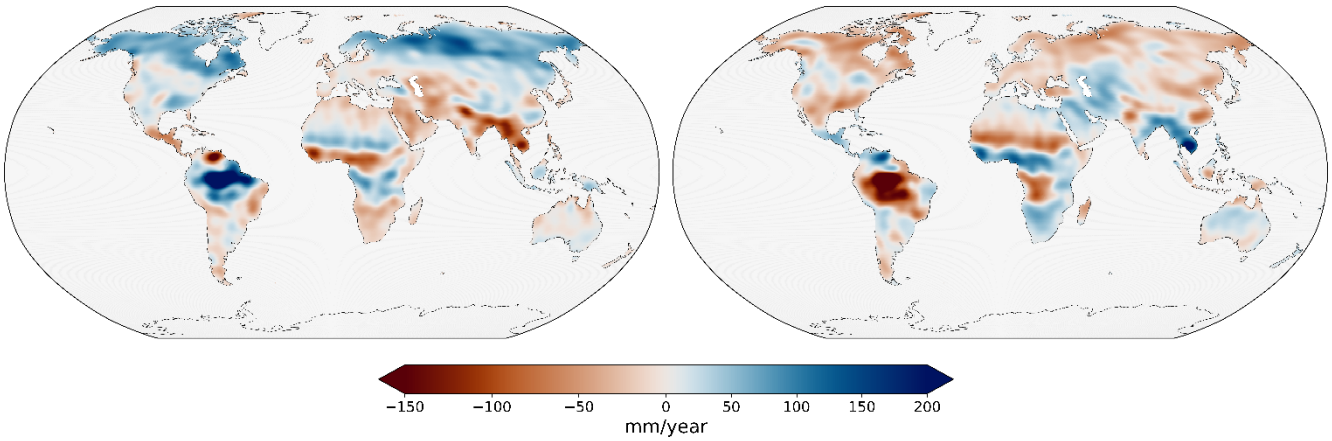

Figure 9: GWSA at the month of globally maximum groundwater storage in May (left plot) and of globally minimum groundwater storage in October (right plot)

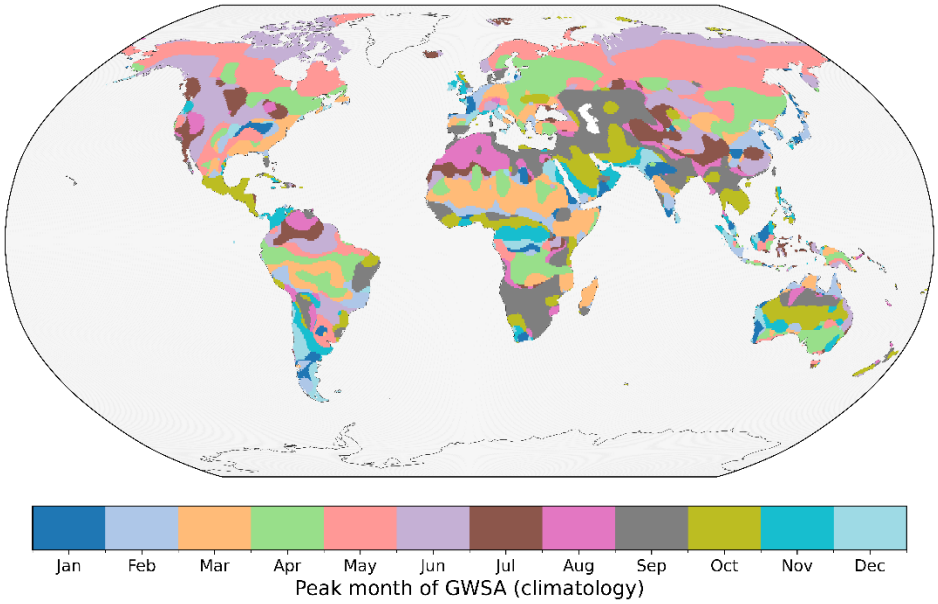

Figure 10: Month with maximum GWSA in the seasonal cycle, according to the GWSA climatology of each 0.5° cell.

The contribution of seasonal groundwater variations to the seasonal TWSA variations varies markedly across the continental area (Fig. 11). The contribution was calculated by a dimensionless metric, the component contribution ratio (*CCR*) following Eq. 9:

$$CCR_{GWSA,seasonal} = \frac{max(GWSA_{m=1,12}) - min(GWSA_{m=1,12})}{max(TWSA_{mm=1,12}) - min(TWSA_{m=1,12})} * 100 \quad (9)$$

where *max* and *min* are the maximum and minimum monthly water storage anomalies of the GWSA and TWSA monthly climatologies, respectively. Basically, the contribution values should be in the range of up to 100%. However, the calculated variability of groundwater storage exceeds that of TWSA in several regions worldwide (Fig. 11), in particular in dry regions of Africa, Middle East, Australia and Central and Eastern Asia, where the absolute seasonal amplitude of GWSA is small (compare Fig. 7). In these regions the *CCR* results need to be taken with caution as they tend to heavily impacted by the uncertainty of the involved WSCs and of TWSA, being at least as large as the storage signal itself.

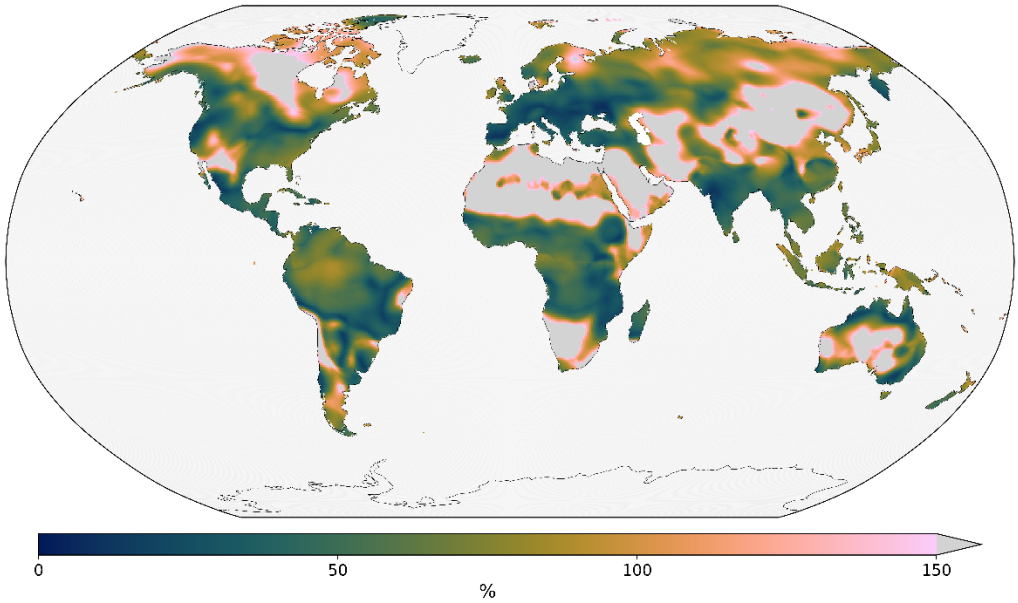

Figure 11: Average contribution of seasonal variations of groundwater storage to the seasonal TWSA variations, as represented by the *CCR* (equation 8).

The linear GWSA trends for the G3P data period from 10/2002 to 09/2023, computed by linear least squares regression, are shown in Fig. 12. Large negative trends show up in regions that have been identified as areas with over-exploitation of groundwater resources in previous studies (see introduction) such as California, the Middle East, northern India, and northern China. Positive GWSA trends can be seen in large areas of Africa, parts of Northern Asia and North America. In comparison to the trends of TWSA, major negative trends by glacier melt in Alaska, Northern Canada and Patagonia as well as due to the drying of the Caspian Sea diminish in the GWSA data after the subtraction process of the G3P processing chain. For other parts of the continents, the large-scale spatial patterns of GWSA and TWSA trends are similar. The linear GWSA trend as an average over all continental areas except Greenland and Antarctica is very small, with a value of 0.016 mm/year over the period 10/2002 to 09/2023 (Fig. 13). This result indicates that the regions with human- or climate-driven groundwater depletion are balanced by others that gain in groundwater over the study period. Also Zhang et al. (2026) show with GRACE/-FO data and ERA5-Land data that 48 % of global regions with significant GWS trends (excluding those regions where the trend is caused by melting glaciers and ice shields) exhibit a decline in groundwater storage and 52 % an increase. Zhang et al. (2026) do not provide a global-scale GWS trend estimate, though. A broader discussion of the significance and possible causes of TWSA and GWSA trends in the G3P data set is given in Hohensinn et al. (2026).

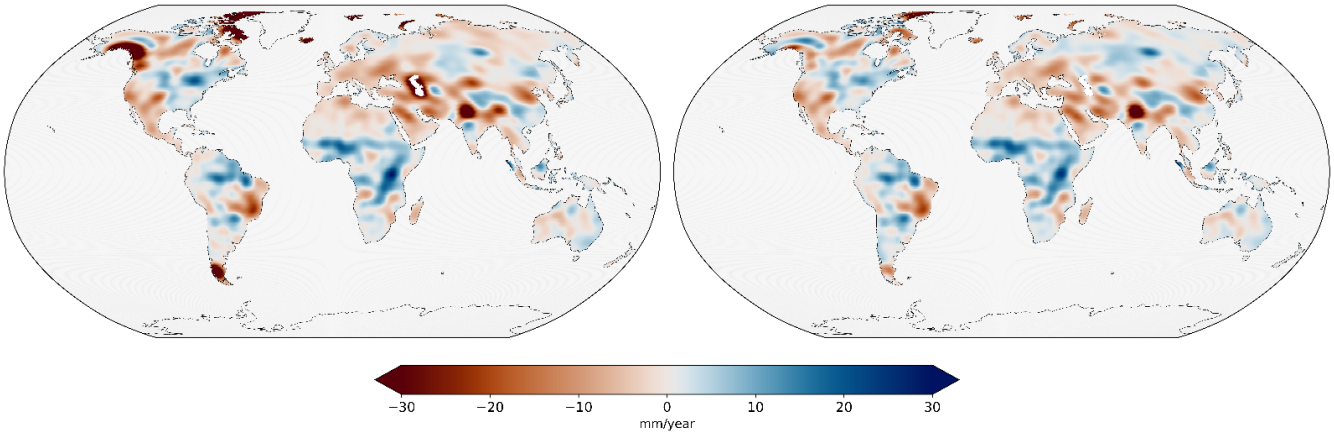

Figure 12: Linear trend of TWSA (left) and GWSA (right) of the G3P data for the period 10/2002 to 09/2023.

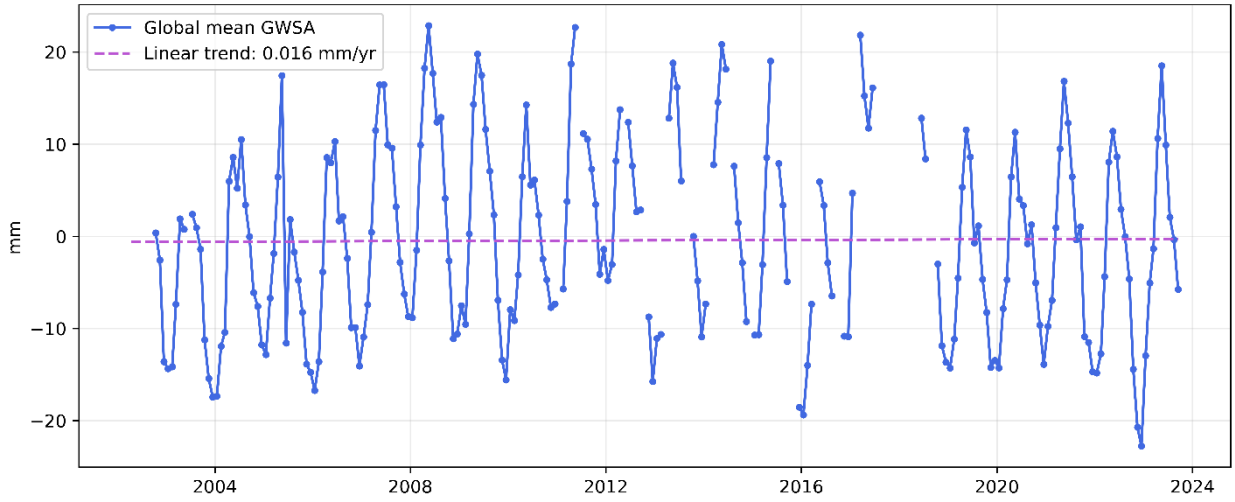

Figure 13: Time series of global mean GWSA (for all continental areas except Greenland and Antarctica) from 10/2002 to 09/2023, with linear trend.

3.3 G3P uncertainties

Figure 14 illustrates the global uncertainty patterns of TWSA and of the WSCs at the 0.5° scale as a temporal mean value over all months in the G3P data set. The time series of the uncertainties of individual WSCs are given as spatial averages over all continental areas in Fig. 15.

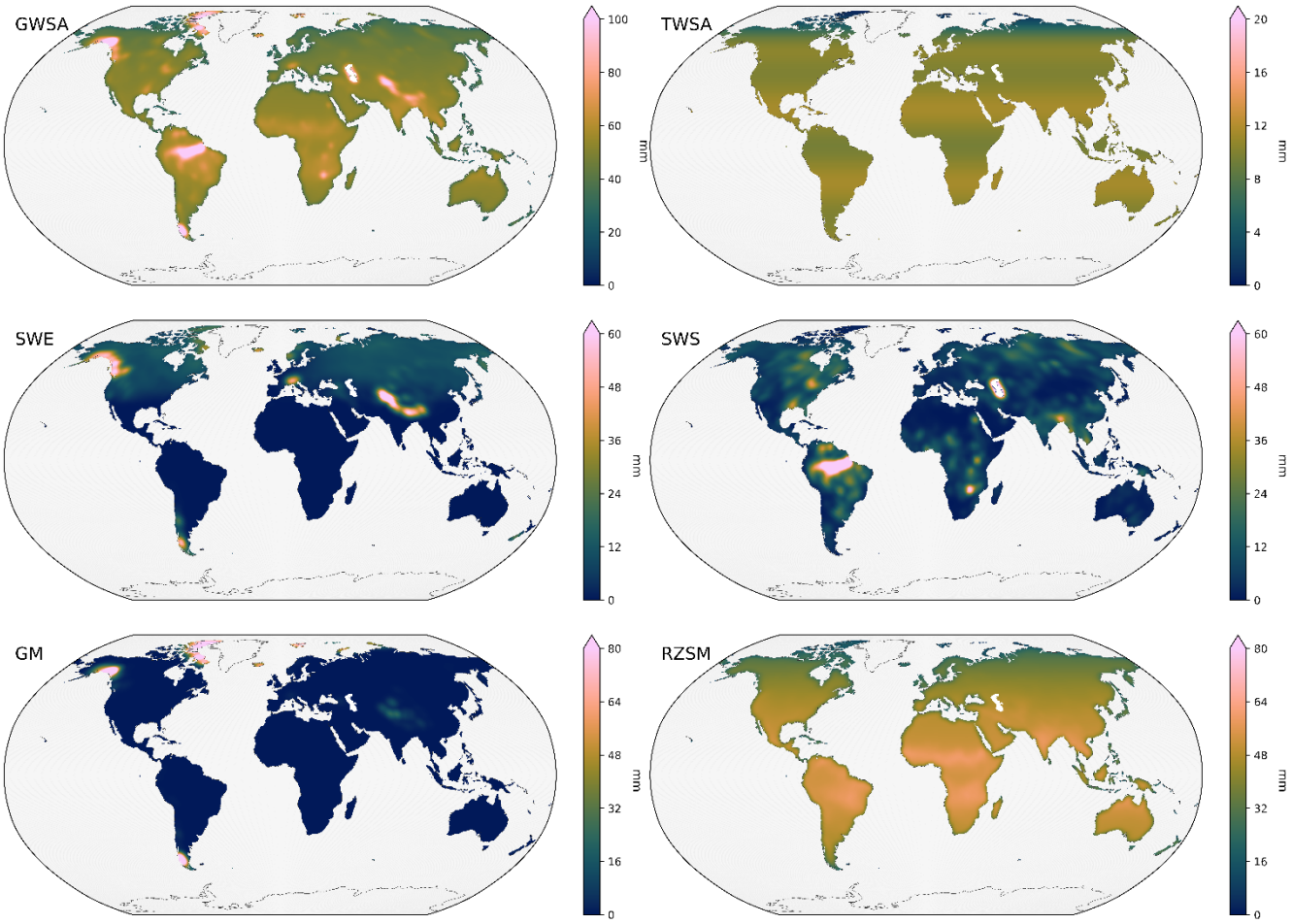

Figure 14: Cell-based (0.5°) monthly uncertainty of the water storage data sets used in G3P, given as a temporal average over the study period 04/2002 to 09/2023. Note the different colour scales of the individual plots.

For the global-average, RZSM exhibits the highest uncertainty, followed by TWSA. TWSA uncertainties tend to decrease towards higher latitudes because of the denser coverage of GRACE/-FO ground tracks and, thus, better resolved gravity field variations. The temporal variability of TWSA uncertainties is comparatively high, with large uncertainties in months with poorly defined gravity fields due to satellite orbit repeat cycles, and in particular towards the end of the GRACE mission in

the years 2015 to 2017 because of system degradation. The uncertainties of snow, surface water storage and glacier mass anomalies are comparatively small in terms of their global averages, but can be higher than those of RZSM and TWSA in spatially confined regions where the respective WSCs are relevant components of the hydrological cycle. These uncertainties also smear out to adjacent areas due to the spatial filtering and smoothing of the WSC data sets (of both the anomalies and their uncertainties) in a GRACE/-FO similar way (see Sect. 2.3.3). The propagated GWSA uncertainties result in a temporal and spatial mean monthly cell-based uncertainty of 52 mm and reflect the spatial patterns of the dominant features of the contributing WSCs, with high uncertainties in and around glaciated and snow-dominated mountainous areas or regions with strong SWS variations. It should be noted that the area-average uncertainties for larger spatial units such as aquifers scale in a reduced way due to the strong and long-ranging covariances of neighbouring grid cell uncertainties.

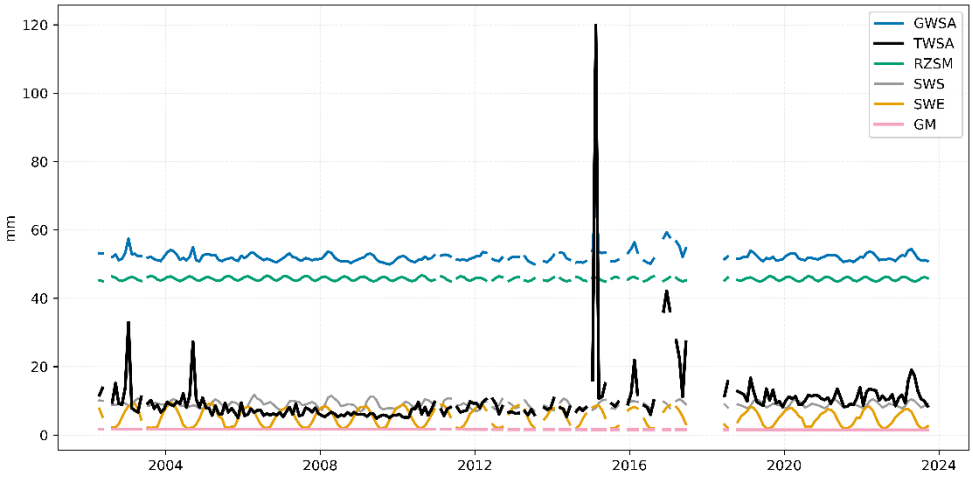

Figure 15: Time series of the uncertainties of the G3P water storage data sets, as global cell-based averages

3.4 Evaluation with in situ groundwater data

Paris Basin

The Paris Basin, located in Northern France, is a multi-layered aquifer system with several main aquifer layers separated by low permeability formations (Contoux et al., 2013). The aquifer system includes unconfined and confined portions, with shallow unconfined aquifers laterally adjacent to or underlain by confined aquifers (Maréchal and Rouillard, 2020). The climate of the basin is temperate oceanic, with an average annual precipitation of around 650 - 900 mm (Habets et al., 2013; Joly et al., 2010). The main aquifers within the basin are highly productive, which have been intensively used for irrigation and water supply of the region (Maréchal and Rouillard, 2020).

The correlation between G3P GWSA and in situ GWLA of the Paris Basin is moderate to strong (r = 0.63), indicating overall moderate agreement in temporal patterns (Table 2; Fig. 16). Both datasets reflect similar interannual and seasonal variations. The in situ data show slightly larger normalized amplitudes at the seasonal scale, while G3P shows more short-term variability. The latter can be related to the uncertainties of the G3P components, in particular of TWSA at this comparatively small spatial scale. Prior to the year of 2013, G3P values tend to be higher than in situ estimates and lower afterwards, possibly related to a stronger negative long-term trend over the study period seen by G3P for the Paris basin.

Table 2: Summary of the aquifer characteristics and correlation analysis

Aquifer	Size (km²)	Hydrogeology	Climate	Main water use	Correlation coefficient
Paris Basin	250.000	Sedimentary rock, mix of unconfined and confined aquifer system	Temperate oceanic	Irrigation and water supply	0.63
High Plains Aquifer	450.000	Unconsolidated sediments, primarily unconfined	Mostly semiarid	Irrigation	0.82
Guarani Aquifer System	1.200.000	Sandstones, mostly confined	Tropical savanna to subtropical	Water supply	0.81

High Plains Aquifer

The High Plains Aquifer, which covers an area of about 450 000 km^2 across eight U.S states, is one of the largest aquifers in the world. It is generally unconfined and consists of unconsolidated sediments of late Tertiary and Quaternary periods (Dennehy, 2000; Strassberg et al., 2009). The climate of the region is mostly semiarid with high evaporation (Strassberg et al., 2007). The aquifer is intensively used for irrigation, accounting for about 30% of groundwater used for irrigation in the US. The correlation coefficient of the two standardized datasets is high (0.82) (Table 2; Fig. 16), suggesting strong agreement between G3P and in situ estimations, with both long-term and seasonal variation patterns being consistent. The correlation is higher before 2016, while after 2016 in situ data show lower values, especially during periods of overall low groundwater storage. For in situ monitored data, groundwater depression cones can occur locally around the pumping wells during pumping periods. The measured groundwater levels with low spatial coverage (Fig. 6) do not necessarily represent the overall condition of the whole aquifer, which may cause discrepancies to the G3P data.

Guarani Aquifer System

The Guarani Aquifer System is a transboundary aquifer of approximately 1.2 million km^2. It is one of the largest groundwater reservoirs in the world, covering parts of Argentina, Brazil, Uruguay and Paraguay. It consists mainly of sandstone formations

overlain by thick Cretaceous basalt flows (Gonçalves et al., 2020; Hirata and Foster, 2021). The aquifer is mostly confined by the underlying and overlying deposits and almost totally storage-dominated with old to very old water (from 4 000 to > 100 000 years) (Hirata and Foster, 2021; Sindico et al., 2018). The climate varies from subtropical in the south to tropical savanna in the north, with precipitation ranging from 1 000 to 1 800 mm/year (Wendland et al., 2006). The aquifer is a strategic source and heavily exploited for the four countries that it covers.

The correlation coefficient of standardized datasets indicates a good positive correlation (0.81) (Table 2; Fig. 16). While the available time period for comparison is comparatively short, the interannual temporal patterns of groundwater storage changes are highly consistent. Regular sub-annual or seasonal variations are not pronounced in either data set. These smooth storage variations in particular for the in situ observations are consistent with the characteristics of a confined aquifer system. The G3P time series additionally exhibits random noise at monthly scales.

In summary, the evaluation case studies presented here demonstrate the applicability of G3P to capture temporal variations in groundwater storage change and its potential value for groundwater assessment across different hydrogeological and climatic settings. All three aquifers exhibit moderate to high correlation between G3P GWSA and in situ GWLA ($r = 0.63 \sim 0.82$), with the High Plains Aquifer and the Guarani Aquifer System showing particularly strong agreement, validating the performance of G3P in both unconfined and confined systems. Observed discrepancies between G3P and in situ time series are not surprising in view of the differences in spatial extent, spacing and resolution of both data sources but also highlight the importance of considering anthropogenic activities (localized pumping effects), aquifer type (recharge or storage dominated) and local heterogeneities when interpreting G3P and in situ monitoring data. Further considerations of G3P evaluation are given in Sect. 5.

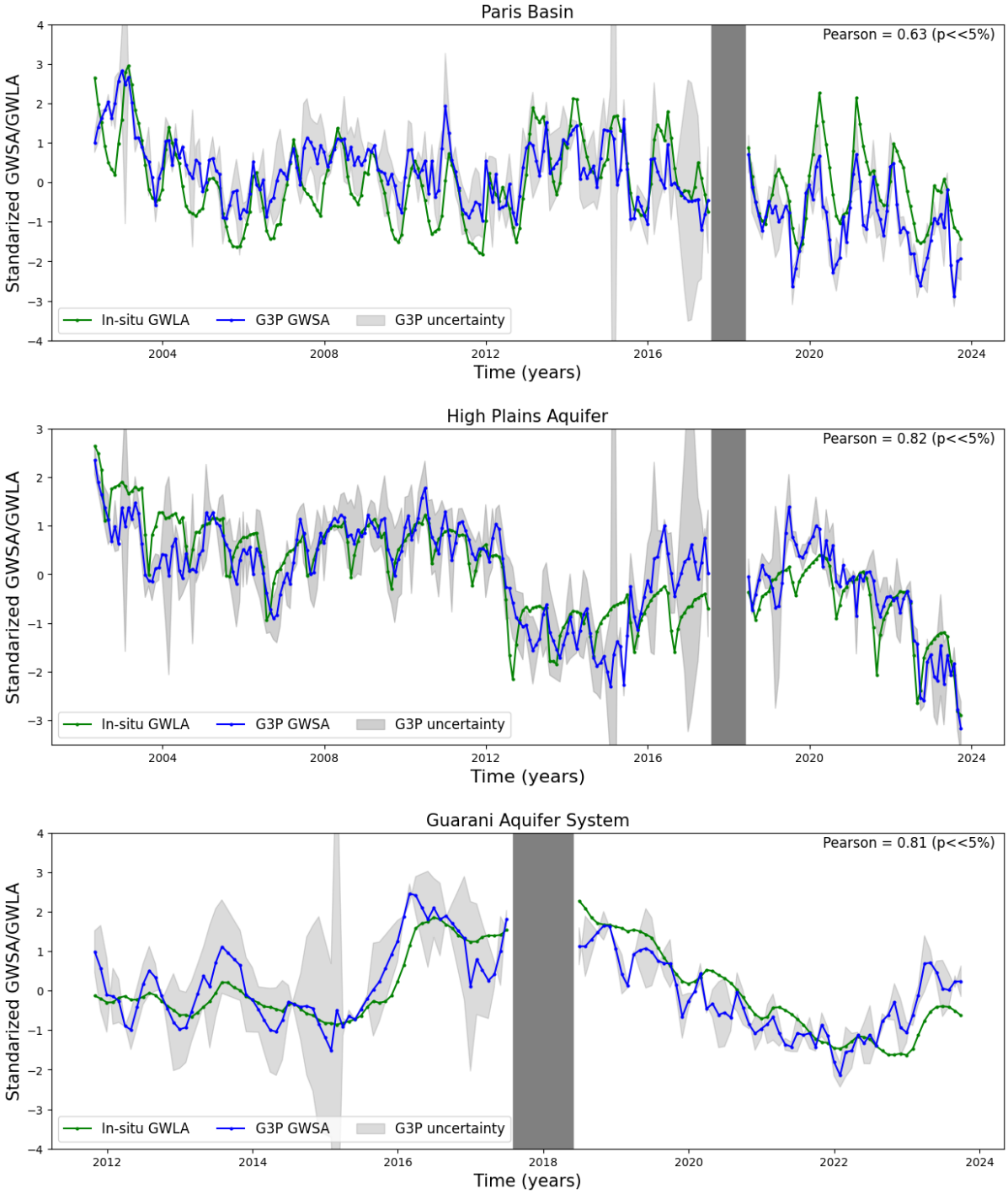

Figure 16: Standardized G3P GWSA and in situ GWLA time series for the three evaluation aquifers. The dark grey period indicates the temporal gap between the GRACE and GRACE-FO missions.

4 Discussion

Following a G3P-like water balance approach in which groundwater storage variations are derived as the residual of total and compartmental terrestrial storage variations is challenging: errors and uncertainties in each component accumulate in the resulting GWSA (e.g., Akl and Thomas (2024), Getirana et al. (2025)) and this needs to be taken into account when interpreting the G3P data. On the other hand, in modelling systems with data assimilation or an offline data merging approach that may alternatively be used to compute GWSA, the water balance (including the storage mass balance) is usually forced to be closed, even if the model is constrained by TWSA and compartmental storage observations. A water balance approach as followed by G3P can thus help elucidate whether the observation-based components match or whether they lead to inconsistencies. A plausibility testing framework (Arifin et al., 2025) to sort out physically plausible combinations of TWSA, GWSA and storage variations of other WSCs, and those that are consistent with hydrological processes, shall also be applied to the G3P data sets. This may ultimately contribute to improving observation systems towards better water balance closure (e.g., Dorigo et al. (2021b)).

The G3P evaluation examples with in situ observations presented in this paper show the adequacy of G3P to represent groundwater dynamics in the selected aquifers under different climate and hydrogeological conditions. Nevertheless, these results cannot be generalized. Other studies, using different sets and processing of TWSA and WSC data, have reported lower correlations between in situ data and GRACE-derived groundwater data. This includes, for example, regions with low amplitudes of groundwater storage variations and sub-Artic regions (e.g., Rateb et al. (2020), Rzepecka et al. (2024)). Also, in this study, only standardized time series of in situ groundwater level and G3P-based groundwater storage were compared, which allows for evaluating the temporal dynamics of G3P data only. Further evaluation should compare the groundwater storage variations directly. For this, the hydrogeological parameters specific yield or storage coefficient are needed to convert the in situ groundwater level observations into storage. However, these parameters are rarely available from direct measurements such as pumping tests, for instance, and even less with the sufficient spatial coverage needed for a large-scale comparison to G3P. Nevertheless, specific yield estimates based on general lithological or hydrogeological mapping may provide useful information to perform an evaluation at the level of storage variations, albeit at the expense of higher uncertainties (Sayyadi et al., 2025).

A particular issue to be considered when using TWSA from satellite-gravimetry is the effect of leakage that is inherent to these data due to the GRACE/-FO observation principles and the need for filtering to reduce noise in TWSA data. Leakage causes actual mass changes to be dispersed from their true locations and, eventually, reduced in amplitude or even lost to ocean areas. We point out that G3P does not include a leakage correction or rescaling approach so far. We proceeded in this way in view of the poorly known real spatial and temporal distribution of TWS or groundwater storage variations from independent sources, i.e., in situ observations or hydrological models, on the basis of which a proper rescaling approach could be developed, While

for G3P, GRACE-like filtering of the WSC data sets makes them more consistent with TWSA, leakage and spatially smoothed patterns due to filtering may still impact the ability to adequately close the water balance and to resolve the amplitude of groundwater storage variations. The amplitudes of G3P-based GWSC may underestimate the real variations in some places and overestimate them in others. The larger the study area of interest for which area-average GWSC variations are computed from G3P, the smaller these errors tend to be. Adequate treatment of leakage in TWSA data is subject to ongoing research and debate in the geodetic community (e.g., International Association of Geodesy (IAG) working group on leakage mitigation). Glacier mass change observations which are well constrained in space and independent from satellite gravimetry – such as the GM input data set used for G3P – might provide an interesting test case to further investigate leakage corrections in GRACE products.

Gaps in the G3P data set presented here for the period 02/2002 to 09/2023 amount to 20 individual months due to GRACE/-FO satellite repeat orbits and instrument failures that do not allow for computing the respective monthly gravity fields, and an 11-month gap of TWSA data between the end of the GRACE lifetime and the launch of GRACE-FO. A more severe limitation for many groundwater applications, though, is the coarse spatial resolution of satellite gravimetry and derived products such as G3P, which is partly related to the above-mentioned leakage issue. With markedly increasing uncertainties and inability to discern the water storage signals of areas with less than 200 000 km² in size, the resolution is beyond the scale of aquifers relevant to groundwater resources management (Xu et al., 2023). Nevertheless, the coarse-resolution G3P data can serve as a valuable input for spatial downscaling approaches to regional scales that have emerged during recent years, by making use of a variety of higher resolution auxiliary data and diverse ML techniques (e.g., Kashani and Safavi (2025)).

A limitation of G3P (as with most other groundwater storage products deduced from GRACE/-FO observations) is the shallow integration depth of the soil moisture data (here 2 m) that are used for subtracting the unsaturated zone storage variations from TWSA. Effectively, all deeper water storage variations are assigned to groundwater as the residual, irrespective of whether they are storage variations in a deeper unsaturated zone or real saturated zone, i.e., groundwater variations. The error caused by this simplification can be expected to vary regionally, depending on factors that govern the magnitude of storage variations in the deep unsaturated zone. These primarily are the climatological, soil physical and hydrogeological conditions, and the actual depth to the groundwater table (e.g., Tsypin et al. (2025)). The damping and delay that a deep unsaturated zone may impose on the transfer of the hydro-meteorological forcing from the surface to groundwater recharge often is associated with low-frequency storage dynamics at inter-annual to decadal time scales (Lischeid et al., 2021). Accordingly, these dynamics can become an error component of a G3P-like groundwater storage approach.

The estimation of SSM under conditions that remain unobservable by microwave satellites (e.g., very dense vegetation and frozen soils) and the extrapolation of SSM to RZSM are purely based on direct observations of SSM and simple mathematical formulations. Consequently, the modelling impact is limited. Despite the likelihood of a reduction in gaps due to global

warming and deforestation, and the potentially increased observability of soil moisture under dense canopies by novel observation systems such as CIMR and the P-band radar of Biomass, no observation system will be capable of closing these gaps entirely. Nevertheless, future efforts should concentrate on enhancing the characterizations of uncertainties introduced by extrapolating SSM observations into uncharted data spaces.

Due to the unavailability of adequate observation-based products, the SWS data set required for G3P is fully based on simulation results of a hydrological model, in contrast to the quest for observation-based data for G3P processing. Also, it does not have uncertainty information that is comparable to the observation-based data sets, propagated from instrument noise and processing uncertainties. Comparing the SWS data used in G3P with SWS data derived from multi-satellite observations of surface water extent in combination with a topographic method in the Congo River basin, Kitambo et al. (2025) showed that the difference between the two approaches propagated into the final GWSA estimates in the form of a seasonal phase shift, in spite of similar storage amplitudes. Significant potential for increasing the role of global-scale observation-based SWS products in future is seen (see Papa and Frappart (2021) and Lin and Song (2026) for an overview), including efforts on altimetry-based lake and reservoir storage products such as by Yao et al. (2023) and in GloLakes (Hou et al., 2024), the aforementioned DAHITI and SWOS projects, or based on the lake level data service within C3S (Cdr, 2020). Furthermore, both lake and river observations will probably profit from the current Surface Water and Ocean Topography (SWOT) satellite mission. Combining waterbodies and their SWS from different sources, and lake and reservoir storage in particular, requires a careful and potentially complex data merging scheme to maintain a closed mass balance.

Estimation of SWE over mountain areas with satellite-based passive microwave radiometer data remains challenging, due to orography and highly varying snow depths on small spatial scales, which cannot yet be resolved by current satellite retrievals. The highest relative errors occur at low snow masses, especially with SWE lower than 50 mm. This results in higher SWE retrieval uncertainties at the beginning of the snow season and during snow melt. Lievens et al. (2019) showed promising results in retrieving snow depth based on Sentinel 1 mission data over mountainous areas. New upcoming products on mountainous snow are expected to enhance snow mass estimates for groundwater purposes in those areas. The work by Venäläinen et al. (2021) on considering a dynamic snow density allows for improving SWE retrievals and is realized within the C3S cryosphere project and its new operational SWE products accessible through the Copernicus service.

The main limitations of the glacier product as delivered for G3P includes (i) the scarcity of glaciological in situ observations in regions like High Mountain Asia, Southern Andes, Arctic Canada, and Russian Arctic, (ii) the availability of geodetic observations before the satellite era (less relevant for G3P), (iii) grid point artefacts in polar regions where glaciers size is larger than one grid cell, (iv) differences in the hydrological years across regions (Northern Hemisphere, Tropics, Southern Hemisphere), (v) and the consideration of glacier-specific area changes over time (Dussaillant et al., 2025). Furthermore, limitations on the continuity and future quality of the glacier change product relate mostly to the continuity, spatial and

temporal richness of glacier change observations, with special regard to annual and seasonal (summer-winter) observations from the glaciological (in situ) method used to adjust the sine interpolation, and the continuity of available non-commercial optical and radar satellite missions allowing to enrich the geodetic observation sample (Berthier et al., 2023; Zemp et al., 2025).

5 Data availability

The G3P data described in this paper, corresponding to G3P version 1.12, are accessible via GFZ Data Services at https://doi.org/10.5880/G3P.2024.001 (Güntner et al., 2024). The data set comprises the groundwater storage anomalies themselves as well as the anomalies of all the individual data sets that were used to derive GWSA, i.e., TWSA and the WSCs glacier mass, snow water equivalent, root-zone soil moisture and surface water storage, spatially filtered with a Gaussian filter to be compatible with TWS. For all individual data sets, also the uncertainty information is given. The spatial coverage of the data set is global, except Greenland and Antarctica, with 0.5° resolution. Temporal coverage is from April 2002 to September 2023 with monthly temporal resolution. The gridded data sets are available as netCDF files in netCDF-4 format following CF1.8 standards and contain variables for the storage values as anomalies and of their uncertainties, all in mm equivalent water height. Furthermore, the G3P data can be visualized as global maps on GravIS (Gravity Information Service) (Dahle et al., 2025) at https://gravis.gfz.de/gws. In GravIS, also area-average groundwater storage time series can be generated and visualized for pre-defined spatial units, including large river basins, aquifers, and climatologically similar regions worldwide, and the resulting time series can be downloaded.

The land–ocean masks and land fractions used in the G3P processing are accessible at https://doi.org/10.5880/G3P.2025.001 (Sharifi et al., 2025b). We provide four global masks on WGS84 at 0.1°, 0.25°, 0.5° and 1° resolution as CF-1.8 NetCDF-4 files. The masks follow the G3P v1.12 domain (global excluding Greenland and Antarctica) and the 0.5° mask is the one used for G3P outputs.

6 Conclusions

G3P provides a data set of groundwater storage variations that is consistently processed at the global scale, taking TWSA from satellite gravimetry as its primary input. GWSA is derived by subtracting storage variations of the continental hydrosphere and cryosphere other than groundwater, i.e., glaciers, snow, soil moisture and surface water. Considering these four compartments at the same time and with global coverage is a distinctive feature of G3P. In addition, the compartmental storage variations are largely based on satellite and in situ observations. Furthermore, all WSC data build up on existing Copernicus data sets and services, making G3P a unique cross-cutting combination product. All contributing data sets have been further developed in terms of spatial coverage, depth extent or regional mass change allocation to match G3P requirements. These

developments can be expected to expand the range of applicability of each data set also as a stand-alone product. With respect to gravity-based TWSA, G3P stands out by being based on the COST-G combination product which merges time-variable gravity data sets of several GRACE/-FO processing centres. Thus, different from other groundwater data sets that are derived from a single GRACE TWSA product, G3P takes advantage of a more robust TWSA input because noisy or outlying data points are down-weighted in the combination. Overall, the consistently and comprehensively processed G3P data offer valuable information on global-scale groundwater storage variations that can serve for a better understanding of the Earth's water cycle and its changes, for the assessment of large-scale groundwater resources and for evaluating and constraining hydrological and groundwater models.

The close to zero GWSA trend that we find as the continental average over the study period delivers a new, albeit not necessarily intuitive perspective on the global water cycle. It points out that in spite of the regionally important negative trends due to climate variability and/or climate change and human groundwater use and overexploitation (which often dominate the general perception on the Earth's state of groundwater), many regions worldwide gained groundwater over the study period, leading to globally stable GWS over the last slightly more than two decades. It should be noted, though, that the available record is still too short to discern the effects of longer-term natural climate variability and those of climate change.

Evaluation examples of G3P against in situ observations of groundwater level variations showed reasonable performance for the selected large-scale aquifers. However, many more G3P evaluation studies under varying environmental conditions are needed to further assess the performance of G3P and, ultimately, to improve it. Thus, we explicitly encourage users to report their results of G3P applications, including poorly performing outcomes.

While G3P processing strives for the use of observed data as far as possible, the current capabilities of observing technologies require complementary quantification of storage variations in space and/or time by modelling approaches. For G3P, this encompasses data from hydrological and land surface models for (i) snow water equivalent in mountainous regions and for the southern hemisphere and (ii) surface water storage for all water bodies (except for the Caspian Sea for which observations from satellite altimetry are used). For RZSM in areas with dense vegetation cover or under frozen conditions, and for extrapolating from surface soil moisture to larger soil depths, interpolation and depth-scaling methods are applied that are purely driven by the direct soil moisture observations and thus different from the model-based approaches for SWE and SWS. As discussed in Sec. 4, advances in remote sensing techniques, retrieval methods and product generation may deliver even more and improved observation-based components for the G3P processing chain, while the continuity of high-quality ground-based as well as satellite-based observing systems is pivotal.

For TWSA from satellite gravimetry, limitations of GRACE/-FO with respect to spatial resolution may be alleviated to some extent by new constellations of future satellite gravity missions (e.g., Daras et al. (2024)). The approved funding for the

successor mission GRACE-Continuity (GRACE-C) gives prospect for extending G3P into a long-term climate data record (CDR). In this respect, G3P has been developed as a prototype for an operational global groundwater service. While the European Union's Earth Observation Programme Copernicus already provides many operational services of CDRs, one for the ECV groundwater has not been available until now. G3P is about to be further developed into a new operational data service within the Copernicus Climate Change Service C3S, as a cross-cutting approach that combines and adapts the existing operational Copernicus products for individual storage compartments.

Finally, it is important to emphasize that G3P and other satellite-derived groundwater products cannot serve as substitutes for in situ monitoring. In situ data remain essential for capturing small-scale spatial variations and short-term fluctuations in groundwater levels, which are often beyond the resolution of satellite-based estimates. In situ data are essential for the ground-based evaluation of the satellite-based estimates. In turn, G3P can serve as a valuable supplement for in situ data in data-scarce regions. At best, satellite-derived and in situ monitored groundwater data can complement each other and improve the robustness of groundwater resources assessments, supporting water cycle analyses and sustainable water management at regional and global scales.

Competing interests

The authors declare that they have no conflict of interest.

Author contribution

AG conceptualized the study and data set development and secured funding. ES and JH developed and coded the G3P data combination scheme and produced the groundwater data. EB, CD, ND, HD, FF, AJ, ML and UM produced the different levels of gravity data, ID and MZ produced the glacier data, MK and KL produced the snow data, WD, AP and WP produced the soil moisture data, JH and EB produced the surface water data, FC and CTV carried out the evaluation analyses. AG wrote and prepared the manuscript with text and graphics contributions from all co-authors. All co-authors revised the full manuscript.

Acknowledgements

G3P was funded by the EU Horizon 2020 programme in response to the call LC-SPACE-04-EO-2019-2020 "Copernicus evolution – Research activities in support of cross-cutting applications between Copernicus services" under grant agreement No. 870353. GloFAS v4.0 output and state variables were kindly provided by the Joint Research Centre (JRC) of the European Commission and the European Centre for Medium-Range Weather Forecasts (ECMWF). Lake altimetry data for the Caspian

Sea was kindly provided by Christian Schwatke of the DAHITI project. I.D. and M.Z. acknowledge support from the Swiss Federal Office of Meteorology and Climatology (MeteoSwiss) within the framework of GCOS Switzerland, the European Space Agency (ESA) project GlaMBIE (4000138018/22/I-DT), the EU H2020 project G3P (870353), and the EU Copernicus Climate Change Service (C3S). We thank the German Space Operations Center (GSOC) of the German Aerospace Center (DLR) for providing continuously and nearly 100% of the raw telemetry data of the twin GRACE satellites.

References

Abich, K., Abramovici, A., Amparan, B., Baatzsch, A., Okihiro, B. B., Barr, D. C., Bize, M. P., Bogan, C., Braxmaier, C., Burke, M. J., Clark, K. C., Dahl, C., Dahl, K., Danzmann, K., Davis, M. A., de Vine, G., Dickson, J. A., Dubovitsky, S., Eckardt, A., Ester, T., Barranco, G. F., Flatscher, R., Flechtner, F., Folkner, W. M., Francis, S., Gilbert, M. S., Gilles, F., Gohlke, M., Grossard, N., Guenther, B., Hager, P., Hauden, J., Heine, F., Heinzel, G., Herding, M., Hinz, M., Howell, J., Katsumura, M., Kaufer, M., Klipstein, W., Koch, A., Kruger, M., Larsen, K., Lebeda, A., Lebeda, A., Leikert, T., Liebe, C. C., Liu, J., Lobmeyer, L., Mahrdt, C., Mangoldt, T., McKenzie, K., Misfeldt, M., Morton, P. R., Müller, V., Murray, A. T., Nguyen, D. J., Nicklaus, K., Pierce, R., Ravich, J. A., Reavis, G., Reiche, J., Sanjuan, J., Schütze, D., Seiter, C., Shaddock, D., Sheard, B., Sileo, M., Spero, R., Spiers, G., Stede, G., Stephens, M., Sutton, A., Trinh, J., Voss, K., Wang, D., Wang, R. T., Ware, B., Wegener, H., Windisch, S., Woodruff, C., Zender, B., and Zimmermann, M.: In-Orbit Performance of the GRACE Follow-on Laser Ranging Interferometer, Physical Review Letters, 123, https://doi.org/10.1103/PhysRevLett.123.031101, 2019.

Adams, K. H., Reager, J. T., Rosen, P., Wiese, D. N., Farr, T. G., Rao, S., Haines, B. J., Argus, D. F., Liu, Z., Smith, R., Famiglietti, J. S., and Rodell, M.: Remote Sensing of Groundwater: Current Capabilities and Future Directions, Water Resources Research, 58, https://doi.org/10.1029/2022wr032219, 2022.

Akl, M. and Thomas, B. F.: Challenges in applying water budget framework for estimating groundwater storage changes from GRACE observations, J. Hydrol., 639, https://doi.org/10.1016/j.jhydrol.2024.131600, 2024.

Albergel, C., Rudiger, C., Pellarin, T., Calvet, J. C., Fritz, N., Froissard, F., Suquia, D., Petitpa, A., Piguet, B., and Martin, E.: From near-surface to root-zone soil moisture using an exponential filter: an assessment of the method based on in-situ observations and model simulations, Hydrol. Earth. Sys Sci., 12, 1323-1337, https://doi.org/10.5194/hess-12-1323-2008, 2008.

Ali, S., Wang, Q. M., Liu, D., Fu, Q., Rahaman, M. M., Faiz, M. A., and Cheema, M. J. M.: Estimation of spatio-temporal groundwater storage variations in the Lower Transboundary Indus Basin using GRACE satellite, J. Hydrol., 605, https://doi.org/10.1016/j.jhydrol.2021.127315, 2022.

Arifin, A., Shamsudduha, M., Ramdhan, A. M., Rateb, A., Scanlon, B. R., Setiawan, T., Iman, M. I., Husna, A., and Taylor, R. G.: Plausibility Criteria for GRACE-Derived Groundwater Storage Changes From Aquifers Globally, Geophysical Research Letters, 52, https://doi.org/10.1029/2025gl118580, 2025.

Behzadpour, S., Mayer-Gürr, T., and Krauss, S.: GRACE Follow-On Accelerometer Data Recovery, J. Geophys. Res.-Solid Earth, 126, 10.1029/2020jb021297, 2021.

Berthier, E., Floriciou, D., Gardner, A. S., Gourmelen, N., Jakob, L., Paul, F., Treichler, D., Wouters, B., Belart, J. M. C., Dehecq, A., Dussaillant, I., Hugonnet, R., Kääb, A., Krieger, L., Pálsson, F., and Zemp, M.: Measuring glacier mass changes from space-a review, Reports on Progress in Physics, 86, https://doi.org/10.1088/1361-6633/acaf8e, 2023.

Bierkens, M. F. P. and Wada, Y.: Non-renewable groundwater use and groundwater depletion: a review, Environ. Res. Lett., 14, https://doi.org/10.1088/1748-9326/ab1a5f, 2019.

Boergens, E., Dobslaw, H., Dill, R., Thomas, M., Dahle, C., Murböck, M., and Flechtner, F.: Modelling spatial covariances for terrestrial water storage variations verified with synthetic GRACE-FO data, GEM - International Journal on Geomathematics, 11, 24, https://doi.org/10.1007/s13137-020-00160-0, 2020.

Boergens, E., Kvas, A., Eicker, A., Dobslaw, H., Schawohl, L., Dahle, C., Murbock, M., and Flechtner, F.: Uncertainties of GRACE-Based Terrestrial Water Storage Anomalies for Arbitrary Averaging Regions, J. Geophys. Res.-Solid Earth, 127, https://doi.org/10.1029/2021jb022081, 2022.

Bojinski, S., Verstraete, M., Peterson, T. C., Richter, C., Simmons, A., and Zemp, M.: The concept of essential climate variables in support of climate research, applications, and policy, Bulletin of the American Meteorological Society, 95, 1431-1443, https://doi.org/10.1175/bams-d-13-00047.1, 2014.

Brown, R. D., Fang, B., and Mudryk, L.: Update of Canadian Historical Snow Survey Data and Analysis of Snow Water Equivalent Trends, 1967-2016 RESEARCH NOTE, Atmosphere-Ocean, 57, 149-156, https://doi.org/10.1080/07055900.2019.1598843, 2019.

Bulygina, O. N., Groisman, P. Y., Razuvaev, V. N., and Korshunova, N. N.: Changes in snow cover characteristics over Northern Eurasia since 1966, Environ. Res. Lett., 6, https://doi.org/10.1088/1748-9326/6/4/045204, 2011.

C3S CDR: Lake water levels from 1992 to present derived from satellite observation [dataset], https://doi.org/10.24381/cds.5714c668, 2020.

C3S CDR: Glaciers distribution data from the Randolph Glacier Inventory for year 2000 [dataset], https://doi.org/10.24381/cds.553f1387 2024.

Chandanpurkar, H. A., Famiglietti, J. S., Gopalan, K., Wiese, D. N., Wada, Y., Kakinuma, K., Reager, J. T., and Zhang, F.: Unprecedented continental drying, shrinking freshwater availability, and increasing land contributions to sea level rise, Science Advances, 11, https://doi.org/10.1126/sciadv.adx0298, 2025.

Chen, J. L., Famiglietti, J. S., Scanlon, B. R., and Rodell, M.: Groundwater Storage Changes: Present Status from GRACE Observations, Surveys in Geophysics, 37, 397-417, https://doi.org/10.1007/s10712-015-9332-4, 2016.

Choulga, M., Moschini, F., Mazzetti, C., Grimaldi, S., Disperati, J., Beck, H., Salamon, P., and Prudhomme, C.: Technical note: Surface fields for global environmental modelling, Hydrol. Earth. Sys Sci., 28, 2991-3036, https://doi.org/10.5194/hess-28-2991-2024, 2024.

Collischonn, W., Allasia, D., Da Silva, B. C., and Tucci, C. E. M.: The MGB-IPH model for large-scale rainfall-runoff modelling, Hydrol. Sci. J.-J. Sci. Hydrol., 52, 878-895, https://doi.org/10.1623/hysj.52.5.878, 2007.

Contoux, C., Violette, S., Vivona, R., Goblet, P., and Patriarche, D.: How basin model results enable the study of multi-layer aquifer response to pumping: the Paris Basin, France, Hydrogeology Journal, 21, 545-557, https://doi.org/10.1007/s10040-013-0955-6, 2013.

Crétaux, J. F., Bergé-Nguyen, M., Calmant, S., Jamangulova, N., Satylkanov, R., Lyard, F., Perosanz, F., Verron, J., Montazem, A. S., Le Guilcher, G., Leroux, D., Barrie, J., Maisongrande, P., and Bonnefond, P.: Absolute Calibration or Validation of the Altimeters on the Sentinel-3A and the Jason-3 over Lake Issykkul (Kyrgyzstan), Remote Sensing, 10, https://doi.org/10.3390/rs10111679, 2018.

Cuthbert, M. O., Gleeson, T., Moosdorf, N., Befus, K. M., Schneider, A., Hartmann, J., and Lehner, B.: Global patterns and dynamics of climate-groundwater interactions, Nature Climate Change, 9, 137-+, https://doi.org/10.1038/s41558-018-0386-4, 2019.

Dahle, C., Boergens, E., Sasgen, I., Döhne, T., Reissland, S., Dobslaw, H., Klemann, V., Murböck, M., König, R., Dill, R., Sips, M., Sylla, U., Groh, A., Horwath, M., and Flechtner, F.: GravIS: mass anomaly products from satellite gravimetry, Earth System Science Data, 17, 611-631, https://doi.org/10.5194/essd-17-611-2025, 2025.

Daras, I., March, G., Pail, R., Hughes, C. W., Braitenberg, C., Güntner, A., Eicker, A., Wouters, B., Heller-Kaikov, B., Pivetta, T., and Pastorutti, A.: Mass-change And Geosciences International Constellation (MAGIC) expected impact on science and applications, Geophysical Journal International, 236, 1288-1308, https://doi.org/10.1093/gji/ggad472, 2024.

De Santis, D. and Biondi, D.: Error Propagation from Remotely Sensed Surface Soil Moisture Into Soil Water Index Using an Exponential Filter, HIC 2018. 13th International Conference on Hydroinformatics, 520-525, https://doi.org/10.29007/kvhb.

Dennehy, K. F.: High Plains regional ground-water study (No. 091–00), Fact Sheet., U.S. Geological Survey, https://doi.org/10.3133/fs09100, 2000.

Dobslaw, H., Bergmann-Wolf, I., Dill, R., Poropat, L., Thomas, M., Dahle, C., Esselborn, S., König, R., and Flechtner, F.: A new high-resolution model of non-tidal atmosphere and ocean mass variability for de-aliasing of satellite gravity observations: AOD1B RL06, Geophysical Journal International, 211, 263-269, https://doi.org/10.1093/gji/ggx302, 2017.

Dorigo, W., Preimesberger, W., Reimer, C., Van der Schalie, R., Pasik, A., De Jeu, R., and Paulik, C.: Soil moisture gridded data from 1978 to present, Copernicus Climate Change Service (C3S) Climate Data Store (CDS) [dataset], https://doi.org/10.24381/cds.d7782f18 2018.

Dorigo, W., Dietrich, S., Aires, F., Brocca, L., Carter, S., Cretaux, J. F., Dunkerley, D., Enomoto, H., Forsberg, R., Güntner, A., Hegglin, M. I., Hollmann, R., Hurst, D. F., Johannessen, J. A., Kummerow, C., Lee, T., Luojus, K., Looser, U., Miralles, D. G., Pellet, V., Recknagel, T., Vargas, C. R., Schneider, U., Schoeneich, P., Schröder, M., Tapper, N., Vuglinsky, V., Wagner, W., Yu, L. S., Zappa, L., Zemp, M., and Aich, V.: Closing the Water Cycle from Observations across Scales: Where Do We Stand?, Bulletin of the American Meteorological Society, 102, E1897-E1935, https://doi.org/10.1175/bams-d-19-0316.1, 2021a.

Dorigo, W., Himmelbauer, I., Aberer, D., Schremmer, L., Petrakovic, I., Zappa, L., Preimesberger, W., Xaver, A., Annor, F., Ardo, J., Baldocchi, D., Bitelli, M., Bloschl, G., Bogena, H., Brocca, L., Calvet, J. C., Camarero, J. J., Capello, G., Choi, M., Cosh, M. C., van de Giesen, N., Hajdu, I., Ikonen, J., Jensen, K. H., Kanniah, K. D., de Kat, I., Kirchengast, G., Rai, P. K., Kyrouac, J., Larson, K., Liu, S. X., Loew, A., Moghaddam, M., Fernandez, J. M., Bader, C. M., Morbidelli, R., Musial, J. P., Osenga, E., Palecki, M. A., Pellarin, T., Petropoulos, G. P., Pfeil, I., Powers, J., Robock, A., Rudiger, C., Rummel, U., Strobel, M., Su, Z. B., Sullivan, R., Tagesson, T., Varlagin, A., Vreugdenhil, M., Walker, J., Wen, J., Wenger, F., Wigneron, J. P., Woods, M., Yang, K., Zeng, Y. J., Zhang, X., Zreda, M., Dietrich, S., Gruber, A., van Oevelen, P., Wagner, W., Scipal, K., Drusch, M., and Sabia, R.: The International Soil Moisture Network: serving Earth system science for over a decade, Hydrol. Earth. Sys Sci., 25, 5749-5804, https://doi.org/10.5194/hess-25-5749-2021, 2021b.

Dussaillant, I., Bannwart, J., Paul, F., and Zemp, M.: Glacier mass change global gridded data from 1976 to present derived from the Fluctuations of Glaciers Database. World Glacier Monitoring Service. [dataset], https://doi.org/10.24381/cds.ba597449, 2023.

Dussaillant, I., Hugonnet, R., Huss, M., Berthier, E., Bannwart, J., Paul, F., and Zemp, M.: Annual mass change of the world's glaciers from 1976 to 2024 by temporal downscaling of satellite data with in situ observations, Earth System Science Data, 17, 1977-2006, https://doi.org/10.5194/essd-17-1977-2025, 2025.

Fan, Y., Miguez-Macho, G., Jobbágy, E. G., Jackson, R. B., and Otero-Casal, C.: Hydrologic regulation of plant rooting depth, Proc. Natl. Acad. Sci. U. S. A., 114, 10572-10577, https://doi.org/10.1073/pnas.1712381114, 2017.

Flechtner, F., Neumayer, K. H., Dahle, C., Dobslaw, H., Fagiolini, E., Raimondo, J. C., and Guntner, A.: What Can be Expected from the GRACE-FO Laser Ranging Interferometer for Earth Science Applications?, Surveys in Geophysics, 37, 453-470, https://doi.org/10.1007/s10712-015-9338-y, 2016.

Frappart, F. and Ramillien, G.: Monitoring Groundwater Storage Changes Using the Gravity Recovery and Climate Experiment (GRACE) Satellite Mission: A Review, Remote Sensing, 10, https://doi.org/10.3390/rs10060829, 2018.

Garcia, D.: Robust smoothing of gridded data in one and higher dimensions with missing values, Computational Statistics & Data Analysis, 54, 1167-1178, https://doi.org/10.1016/j.csda.2009.09.020, 2010.

Gelaro, R., McCarty, W., Suárez, M. J., Todling, R., Molod, A., Takacs, L., Randles, C. A., Darmenov, A., Bosilovich, M. G., Reichle, R., Wargan, K., Coy, L., Cullather, R., Draper, C., Akella, S., Buchard, V., Conaty, A., da Silva, A. M., Gu, W., Kim, G. K., Koster, R., Lucchesi, R., Merkova, D., Nielsen, J. E., Partyka, G., Pawson, S., Putman, W., Rienecker, M., Schubert, S. D., Sienkiewicz, M., and Zhao, B.: The Modern-Era Retrospective Analysis for Research and Applications, Version 2 (MERRA-2), J. Climate, 30, 5419-5454, https://doi.org/10.1175/jcli-d-16-0758.1, 2017.

Getirana, A., Kumar, S., and Rodell, M.: Inconsistencies in GRACE-Based Groundwater Storage Estimation-A Call for a Proper Use of Land Surface Models, Geophysical Research Letters, 52, 10.1029/2025gl119197, 2025.

Gleeson, T., Befus, K. M., Jasechko, S., Luijendijk, E., and Cardenas, M. B.: The global volume and distribution of modern groundwater, Nature Geoscience, 9, 161-+, https://doi.org/10.1038/ngeo2590, 2016.

Gonçalves, R. D., Teramoto, E. H., and Chang, H. K.: Regional Groundwater Modeling of the Guarani Aquifer System, Water, 12, https://doi.org/10.3390/w12092323, 2020.

Gruber, A., Scanlon, T., van der Schalie, R., Wagner, W., and Dorigo, W.: Evolution of the ESA CCI Soil Moisture climate data records and their underlying merging methodology, Earth System Science Data, 11, 717-739, https://doi.org/10.5194/essd-11-717-2019, 2019.

Gruber, A., Su, C. H., Zwieback, S., Crowd, W., Dorigo, W., and Wagner, W.: Recent advances in (soil moisture) triple collocation analysis, International Journal of Applied Earth Observation and Geoinformation, 45, 200-211, https://doi.org/10.1016/j.jag.2015.09.002, 2016.

Güntner, A., Schmidt, R., and Döll, P.: Supporting large-scale hydrogeological monitoring and modelling by time-variable gravity data, Hydrogeology Journal, 15, 167-170, https://doi.org/10.1007/s10040-006-0089-1, 2007.

Güntner, A., Sharifi, E., Haas, J., Boergens, E., Dahle, C., Dobslaw, H., Dorigo, W., Dussailant, I., Flechtner, F., Jäggi, A., Kosmale, M., Luojus, K., Mayer-Gürr, T., Meyer, U., Preimesberger, W., Ruz Vargas, C., and Zemp, M.: Global Gravity-based Groundwater Product (G3P) V. 1.12, GFZ Data Services [dataset], https://doi.org/10.5880/g3p.2024.001, 2024.

Guo, X. M., Fang, X. Q., Cao, Y., Yang, L. L., Ren, L. L., Chen, Y. H., and Zhang, X. X.: Reconstruction of ESA CCI soil moisture based on DCT-PLS and in situ soil moisture, Hydrology Research, https://doi.org/10.2166/nh.2022.058, 2022.

Haberkorn, A.: European Snow Booklet – an Inventory of Snow Measurements in Europe, EnviDat [dataset], https://doi.org/10.16904/envidat.59, 2019.

Habets, F., Boé, J., Déqué, M., Ducharne, A., Gascoin, S., Hachour, A., Martin, E., Pagé, C., Sauquet, E., Terray, L., Thiéry, D., Oudin, L., and Viennot, P.: Impact of climate change on the hydrogeology of two basins in northern France, Climatic Change, 121, 771-785, https://doi.org/10.1007/s10584-013-0934-x, 2013.

Hersbach, H., Bell, B., Berrisford, P., Hirahara, S., Horányi, A., Muñoz-Sabater, J., Nicolas, J., Peubey, C., Radu, R., Schepers, D., Simmons, A., Soci, C., Abdalla, S., Abellan, X., Balsamo, G., Bechtold, P., Biavati, G., Bidlot, J., Bonavita, M., De Chiara, G., Dahlgren, P., Dee, D., Diamantakis, M., Dragani, R., Flemming, J., Forbes, R., Fuentes, M., Geer, A., Haimberger, L., Healy, S., Hogan, R. J., Hólm, E., Janisková, M., Keeley, S., Laloyaux, P., Lopez, P., Lupu, C., Radnoti, G., de Rosnay, P., Rozum, I., Vamborg, F., Villaume, S., and Thépaut, J. N.: The ERA5 global reanalysis, Quarterly Journal of the Royal Meteorological Society, 146, 1999-2049, https://doi.org/10.1002/qj.3803, 2020.

Hirata, R. and Foster, S.: The Guarani Aquifer System - from regional reserves to local use, Quarterly Journal of Engineering Geology and Hydrogeology, 54, https://doi.org/10.1144/qjegh2020-091, 2021.

Hirschi, M., Mueller, B., Dorigo, W., and Seneviratne, S. I.: Using remotely sensed soil moisture for land-atmosphere coupling diagnostics: The role of surface vs. root-zone soil moisture variability, Remote Sensing of Environment, 154, 246-252, https://doi.org/10.1016/j.rse.2014.08.030, 2014.

Hohensinn, R., Gou, J., Meyer, U., Humphrey, V., Dorigo, W., Boergens, E., Soja, B., Gruber, A., Jensen, L., Eicker, A., Rast, M., and Güntner, A.: Water storage trends derived from the GRACE/-FO global gravity-based groundwater product (G3P), EGUsphere [preprint], https://doi.org/10.5194/egusphere-2026-975, 2026.

Horvath, A., Murböck, M., Pail, R., and Horwath, M.: Decorrelation of GRACE Time Variable Gravity Field Solutions Using Full Covariance Information, Geosciences, 8, 323, https://doi.org/10.3390/geosciences8090323, 2018.

Hosseini, M. and Kerachian, R.: A data fusion-based methodology for optimal redesign of groundwater monitoring networks, J. Hydrol., 552, 267-282, https://doi.org/10.1016/j.jhydrol.2017.06.046, 2017.

Hou, J. W., Van Dijk, A., Renzullo, L. J., and Larraondo, P. R.: GloLakes: water storage dynamics for 27 000 lakes globally from 1984 to present derived from satellite altimetry and optical imaging, Earth System Science Data, 16, 201-218, https://doi.org/10.5194/essd-16-201-2024, 2024.

Huggins, X., Gleeson, T., Famiglietti, J. S., Reinecke, R., Zamrsky, D., Wagener, T., Taylor, R. G., Konar, M., Vargas, C. R., Porkka, M., Wang-Erlandsson, L., de Graaf, I., Cuthbert, M., Lindersson, S., Wada, Y., Bierkens, M. F. P., Pokhrel, Y., Rocha, J., Baldassarre, G. D., Kummu, M., Ferguson, G., Mukherjee, A., Lo, M. H., Scanlon, B. R., Johnson, M. S., and Zheng, C. M.: A review of open data for studying global groundwater in social-ecological systems, Environ. Res. Lett., 20, https://doi.org/10.1088/1748-9326/adf127, 2025.

Hugonnet, R., McNabb, R., Berthier, E., Menounos, B., Nuth, C., Girod, L., Farinotti, D., Huss, M., Dussaillant, I., Brun, F., and Kääb, A.: Accelerated global glacier mass loss in the early twenty-first century, Nature, 592, 726-+, https://doi.org/10.1038/s41586-021-03436-z, 2021.

IGRAC: The Global Groundwater Monitoring Network (GGMN) [dataset], https://doi.org/10.58154/6Z0Y-DA34, 2025.

Jäggi, A., Meyer, U., Lasser, M., Jenny, B., Lopez, T., Flechtner, F., Dahle, C., Förste, C., Mayer-Gürr, T., Kvas, A., Lemoine, J.-M., Bourgogne, S., Weigelt, M., and Groh, A.: International Combination Service for Time-Variable Gravity Fields (COST-G), in: International Association of Geodesy Symposia, edited by: Freymueller, J. T., and Sánchez, L., Springer International Publishing, Cham, 57–65, 2023.

Jäggi, A., Weigelt, M., Flechtner, F., Güntner, A., Mayer-Gurr, T., Martinis, S., Bruinsma, S., Flury, J., Bourgogne, S., Steffen, H., Meyer, U., Jean, Y., Susnik, A., Grahsl, A., Arnold, D., Cann-Guthauser, K., Dach, R., Li, Z., Chen, Q., van Dam, T., Gruber, C., Poropat, L., Gouweleeuw, B., Kvas, A., Klinger, B., Lemoine, J. M., Biancale, R., Zwenzner, H., Bandikova, T., and Shabanloui, A.: European Gravity Service for Improved Emergency Management (EGSIEM)-from concept to implementation, Geophysical Journal International, 218, 1572-1590, https://doi.org/10.1093/gji/ggz238, 2019.

Jasechko, S., Seybold, H., Perrone, D., Fan, Y., Shamsudduha, M., Taylor, R. G., Fallatah, O., and Kirchner, J. W.: Rapid groundwater decline and some cases of recovery in aquifers globally, Nature, 625, https://doi.org/10.1038/s41586-023-06879-8, 2024.

Jekeli, C.: Alternative Methods to Smooth the Earth's Gravity Field, The Ohio State University. Ohio, 327 pp., 1981.

Joly, D., Brossard, T., Cardot, H., Cavailhes, J., Hilal, M., and Wavresky, P.: Les types de climats en France, une construction spatiale, Cybergeo Eur. J. Geogr, https://doi.org/10.4000/cybergeo.23155, 2010.

Karandish, F., Liu, S. D., and de Graaf, I.: Global groundwater sustainability: A critical review of strategies and future pathways, J. Hydrol., 657, 10.1016/j.jhydrol.2025.133060, 2025.

Kashani, A. and Safavi, H. R.: Assessing groundwater drought in Iran using GRACE data and machine learning, Scientific Reports, 15, https://doi.org/10.1038/s41598-025-99342-9, 2025.

Kitambo, B. M., Wongchuig, S., Tshimanga, R. M., Paris, A., Blazquez, A., Moreira, D., Frappart, F., Fleischmann, A. S., Kileshye, J. M. O., Tourian, M. J., and Papa, F.: Hydrogeological control of groundwater variations in the Congo River Basin revealed by GRACE water storage change decomposition, Journal of Hydrology-Regional Studies, 62, 10.1016/j.ejrh.2025.102810, 2025.

Kuang, X. X., Liu, J. G., Scanlon, B. R., Jiao, J. J., Jasechko, S., Lancia, M., Biskaborn, B. K., Wada, Y., Li, H. L., Zeng, Z. Z., Guo, Z. L., Yao, Y. Y., Gleeson, T., Nicot, J. P., Luo, X., Zou, Y. G., and Zheng, C. M.: The changing nature of groundwater in the global water cycle, Science, 383, https://doi.org/10.1126/science.adf0630, 2024.

Lamarche, C., Santoro, M., Bontemps, S., d'Andrimont, R., Radoux, J., Giustarini, L., Brockmann, C., Wevers, J., Defourny, P., and Arino, O.: Compilation and Validation of SAR and Optical Data Products for a Complete and Global Map of Inland/Ocean Water Tailored to the Climate Modeling Community, Remote Sensing, 9, https://doi.org/10.3390/rs9010036, 2017.

Landerer, F. W. and Swenson, S. C.: Accuracy of scaled GRACE terrestrial water storage estimates, Water Resources Research, 48, https://doi.org/10.1029/2011wr011453, 2012.

Landerer, F. W., Flechtner, F. M., Save, H., Webb, F. H., Bandikova, T., Bertiger, W. I., Bettadpur, S. V., Byun, S. H., Dahle, C., Dobslaw, H., Fahnestock, E., Harvey, N., Kang, Z. G., Kruizinga, G. L. H., Loomis, B. D., McCullough, C., Murbock, M., Nagel, P., Paik, M., Pie, N., Poole, S., Strekalov, D., Tamisiea, M. E., Wang, F. R., Watkins, M. M., Wen, H. Y., Wiese, D. N., and Yuan, D. N.: Extending the Global Mass Change Data Record: GRACE Follow-On Instrument and Science Data Performance, Geophysical Research Letters, 47, https://doi.org/10.1029/2020gl088306, 2020.

Lasser, M.: Noise Modelling for GRACE Follow-On Observables in the Celestial Mechanics Approach, Eidg. Technische Hochschule Zürich, Switzerland, https://www.sgc.ethz.ch/sgc-volumes/sgk-110.pdf, 2023.

Lehner, B. and Döll, P.: Development and validation of a global database of lakes, reservoirs and wetlands, J. Hydrol., 296, 1-22, https://doi.org/10.1016/j.jhydrol.2004.03.028, 2004.

Li, B. L., Rodell, M., Kumar, S., Beaudoing, H. K., Getirana, A., Zaitchik, B. F., de Goncalves, L. G., Cossetin, C., Bhanja, S., Mukherjee, A., Tian, S. Y., Tangdamrongsub, N., Long, D., Nanteza, J., Lee, J., Policelli, F., Goni, I. B., Daira, D., Bila, M., de Lannoy, G., Mocko, D., Steele-Dunne, S. C., Save, H., and Bettadpur, S.: Global GRACE Data Assimilation for Groundwater and Drought Monitoring: Advances and Challenges, Water Resources Research, 55, 7564-7586, https://doi.org/10.1029/2018wr024618, 2019.

Lievens, H., Demuzere, M., Marshall, H. P., Reichle, R. H., Brucker, L., Brangers, I., de Rosnay, P., Dumont, M., Girotto, M., Immerzeel, W. W., Jonas, T., Kim, E. J., Koch, I., Marty, C., Saloranta, T., Schöber, J., and De Lannoy, G. J. M.: Snow depth variability in the Northern Hemisphere mountains observed from space, Nature Communications, 10, https://doi.org/10.1038/s41467-019-12566-y, 2019.

Lin, Y. L. and Song, C. Q.: Monitoring surface water in floodplains by satellites: Progress, challenges, and perspectives, J. Hydrol., 664, 10.1016/j.jhydrol.2025.134458, 2026.

Lischeid, G., Dannowski, R., Kaiser, K., Nützmann, G., Steidl, J., and Stüve, P.: Inconsistent hydrological trends do not necessarily imply spatially heterogeneous drivers, J. Hydrol., 596, https://doi.org/10.1016/j.jhydrol.2021.126096, 2021.

Long, D., Longuevergne, L., and Scanlon, B. R.: Global analysis of approaches for deriving total water storage changes from GRACE satellites, Water Resources Research, 51, 2574-2594, https://doi.org/10.1002/2014wr016853, 2015.

Long, D., Xu, Y., Cui, Y., Cui, Y., Butler, J. J., Dong, L., Wang, L., Liu, D., Wada, Y., Hu, L., Bai, G., Li, B., Wang, S., Nong, X., Cai, Y., Cheng, C., Mu, Y., Qiao, Y., Wang, J., Wang, H., and Scanlon, B. R.: Unprecedented large-scale aquifer recovery through human intervention, Nature Communications, 16, 7296, https://doi.org/10.1038/s41467-025-62719-5, 2025.

Luojus, K., Pulliainen, J., Takala, M., Lemmetyinen, J., Mortimer, C., Derksen, C., Mudryk, L., Moisander, M., Hiltunen, M., Smolander, T., Ikonen, J., Cohen, J., Salminen, M., Norberg, J., Veijola, K., and Venäläinen, P.: GlobSnow v3.0 Northern Hemisphere snow water equivalent dataset, Scientific Data, 8, https://doi.org/10.1038/s41597-021-00939-2, 2021.

Maréchal, J.-C. and Rouillard, J.: Groundwater in France: Resources, Use and Management Issues, in: Sustainable Groundwater Management: A Comparative Analysis of French and Australian Policies and Implications to Other Countries, Global Issues in Water Policy, edited by: Rinaudo, J.-D., Holley, C., Barnett, S., and Montginoul, M., Springer International Publishing, Cham, 17–45, https://doi.org/10.1007/978-3-030-32766-8_2, 2020.

Martens, B., Miralles, D. G., Lievens, H., van der Schalie, R., de Jeu, R. A. M., Fernández-Prieto, D., Beck, H. E., Dorigo, W. A., and Verhoest, N. E. C.: GLEAM v3: satellite-based land evaporation and root-zone soil moisture, Geoscientific Model Development, 10, 1903-1925, https://doi.org/10.5194/gmd-10-1903-2017, 2017.

Mehrnegar, N., Jones, O., Singer, M. B., Schumacher, M., Jagdhuber, T., Scanlon, B. R., Rateb, A., and Forootan, E.: Exploring groundwater and soil water storage changes across the CONUS at 12.5 km resolution by a Bayesian integration of GRACE data into W3RA, Science of the Total Environment, 758, 10.1016/j.scitotenv.2020.143579, 2021.

Meyer, U., Lasser, M., Dahle, C., Förste, C., Behzadpour, S., Koch, and Jäggi, A.: Combined monthly GRACE-FO gravity fields for a Global Gravity-based Groundwater Product, Geophysical Journal International, 236, 456-469, https://doi.org/10.1093/gji/ggad437, 2023.

Mishra, V., Ellenburg, W. L., Markert, K. N., and Limaye, A. S.: Performance evaluation of soil moisture profile estimation through entropy-based and exponential filter models, Hydrol. Sci. J.-J. Sci. Hydrol., 65, 1036-1048, https://doi.org/10.1080/02626667.2020.1730846, 2020.

Muñoz-Sabater, J., Dutra, E., Agustí-Panareda, A., Albergel, C., Arduini, G., Balsamo, G., Boussetta, S., Choulga, M., Harrigan, S., Hersbach, H., Martens, B., Miralles, D. G., Piles, M., Rodríguez-Fernández, N. J., Zsoter, E., Buontempo, C., and Thépaut, J. N.: ERA5-Land: a state-of-the-art global reanalysis dataset for land applications, Earth System Science Data, 13, 4349-4383, https://doi.org/10.5194/essd-13-4349-2021, 2021.

Opie, S., Taylor, R. G., Brierley, C. M., Shamsudduha, M., and Cuthbert, M. O.: Climate-groundwater dynamics inferred from GRACE and the role of hydraulic memory, Earth System Dynamics, 11, 775-791, https://doi.org/10.5194/esd-11-775-2020, 2020.

Papa, F. and Frappart, F.: Surface Water Storage in Rivers and Wetlands Derived from Satellite Observations: A Review of Current Advances and Future Opportunities for Hydrological Sciences, Remote Sensing, 13, 10.3390/rs13204162, 2021.

Pasik, A., Gruber, A., Preimesberger, W., De Santis, D., and Dorigo, W.: Uncertainty estimation for a new exponential-filter-based long-term root-zone soil moisture dataset from Copernicus Climate Change Service (C3S) surface observations, Geoscientific Model Development, 16, 4957-4976, https://doi.org/10.5194/gmd-16-4957-2023, 2023.

Paulik, C., Dorigo, W., Wagner, W., and Kidd, R.: Validation of the ASCAT Soil Water Index using in situ data from the International Soil Moisture Network, International Journal of Applied Earth Observation and Geoinformation, 30, 1-8, https://doi.org/10.1016/j.jag.2014.01.007, 2014.

Peltier, W. R., Argus, D. F., and Drummond, R.: Comment on "An Assessment of the ICE-6G_C (VM5a) Glacial Isostatic Adjustment Model" by Purcell et al, J. Geophys. Res.-Solid Earth, 123, 2019-2028, https://doi.org/10.1002/2016jb013844, 2018.

Preimesberger, W., Stradiotti, P., and Dorigo, W.: ESA CCI Soil Moisture GAPFILLED: an independent global gap-free satellite climate data record with uncertainty estimates, Earth System Science Data, 17, 4305-4329, https://doi.org/10.5194/essd-17-4305-2025, 2025.

Pulliainen, J.: Mapping of snow water equivalent and snow depth in boreal and sub-arctic zones by assimilating space-borne microwave radiometer data and ground-based observations, Remote Sensing of Environment, 101, 257-269, https://doi.org/10.1016/j.rse.2006.01.002, 2006.

Pulliainen, J., Luojus, K., Derksen, C., Mudryk, L., Lemmetyinen, J., Salminen, M., Ikonen, J., Takala, M., Cohen, J., Smolander, T., and Norberg, J.: Patterns and trends of Northern Hemisphere snow mass from 1980 to 2018, Nature, 581, 294-+, https://doi.org/10.1038/s41586-020-2258-0, 2020.

Rateb, A., Scanlon, B. R., Pool, D. R., Sun, A., Zhang, Z. Z., Chen, J. L., Clark, B., Faunt, C. C., Haugh, C. J., Hill, M., Hobza, C., McGuire, V. L., Reitz, M., Schmied, H. M., Sutanudjaja, E. H., Swenson, S., Wiese, D., Xia, Y. L., and Zell, W.: Comparison of Groundwater Storage Changes From GRACE Satellites With Monitoring and Modeling of Major US Aquifers, Water Resources Research, 56, https://doi.org/10.1029/2020wr027556, 2020.

RGI: Randolph Glacier Inventory - a dataset of global glacier outlines: version 6.0, technical report. Global Land Ice Measurements from Space [dataset], https://doi.org/10.7265/N5-RGI-60, 2017.

Rzepecka, Z., Birylo, M., Jarsjö, J., Cao, F. F., and Pietron, J.: Groundwater Storage Variations across Climate Zones from Southern Poland to Arctic Sweden: Comparing GRACE-GLDAS Models with Well Data, Remote Sensing, 16, 10.3390/rs16122104, 2024.

Saccò, M., Mammola, S., Altermatt, F., Alther, R., Bolpagni, R., Brancelj, A., Brankovits, D., Fiser, C., Gerovasileiou, V., Griebler, C., Guareschi, S., Hose, G. C., Korbel, K., Lictevout, E., Malard, F., Martínez, A., Niemiller, M. L., Robertson, A., Tanalgo, K. C., Bichuette, M. E., Borko, S., Brad, T., Campbell, M. A., Cardoso, P., Celico, F., Cooper, S. J. B., Culver, D., Di Lorenzo, T., Galassi, D. M. P., Guzik, M. T., Hartland, A., Humphreys, W. F., Ferreira, R. L., Lunghi, E., Nizzoli, D., Perina, G., Raghavan, R., Richards, Z., Reboleira, A., Rohde, M. M., Fernández, D. S., Schmidt, S. I., van der Heyde, M., Weaver, L., White, N. E., Zagmajster, M., Hogg, I., Ruhi, A., Gagnon, M. M., Allentoft, M. E., and Reinecke, R.: Groundwater is a hidden global keystone ecosystem, Global Change Biology, 30, https://doi.org/10.1111/gcb.17066, 2024.

Sayer, A. M., Govaerts, Y., Kolmonen, P., Lipponen, A., Luffarelli, M., Mielonen, T., Patadia, F., Popp, T., Povey, A. C., Stebel, K., and Witek, M. L.: A review and framework for the evaluation of pixel-level uncertainty estimates in satellite aerosol remote sensing, Atmospheric Measurement Techniques, 13, 373-404, https://doi.org/10.5194/amt-13-373-2020, 2020.

Sayyadi, S., Nguyen, V. D., Apel, H., Haas, J., Dang, T. T., Than, V. D., Nguyen, N. H., and Güntner, A.: Observation-based analysis of groundwater storage in Vietnam's Central Highlands: influence of hydro-climatic variability, Hydr. Sci. J., https://doi.org/10.1080/02626667.2025.2568558, 2025.

Scanlon, B. R., Fakhreddine, S., Rateb, A., de Graaf, I., Famiglietti, J., Gleeson, T., Grafton, R. Q., Jobbagy, E., Kebede, S., Kolusu, S. R., Konikow, L. F., Long, D., Mekonnen, M., Schmied, H. M., Mukherjee, A., MacDonald, A., Reedy, R. C., Shamsudduha, M., Simmons, C. T., Sun, A. L., Taylor, R. G., Villholth, K. G., Vörösmarty, C., and Zheng, C. M.: Global water resources and the role of groundwater in a resilient water future, Nature Reviews Earth & Environment, 4, 87-101, https://doi.org/10.1038/s43017-022-00378-6, 2023.

Schmied, H. M., Cáceres, D., Eisner, S., Flörke, M., Herbert, C., Niemann, C., Peiris, T. A., Popat, E., Portmann, F. T., Reinecke, R., Schumacher, M., Shadkam, S., Telteu, C. E., Trautmann, T., and Döll, P.: The global water resources and use model WaterGAP v2.2d: model description and evaluation, Geoscientific Model Development, 14, 1037-1079, https://doi.org/10.5194/gmd-14-1037-2021, 2021.

Schwatke, C., Dettmering, D., Bosch, W., and Seitz, F.: DAHITI - an innovative approach for estimating water level time series over inland waters using multi-mission satellite altimetry, Hydrol. Earth. Sys Sci., 19, 4345-4364, https://doi.org/10.5194/hess-19-4345-2015, 2015.

Shamsudduha, M. and Taylor, R. G.: Groundwater storage dynamics in the world's large aquifer systems from GRACE: uncertainty and role of extreme precipitation, Earth System Dynamics, 11, 755-774, https://doi.org/10.5194/esd-11-755-2020, 2020.

Shangguan, Y. L., Min, X. X., and Shi, Z.: Gap Filling of the ESA CCI Soil Moisture Data Using a Spatiotemporal Attention-Based Residual Deep Network, IEEE J. Sel. Top. Appl. Earth Observ. Remote Sens., 16, 5344-5354, https://doi.org/10.1109/jstars.2023.3284841, 2023.

Sharifi, E., Haas, J., Boergens, E., and Güntner, A.: Global Multi-Resolution Land Fraction and Land–Ocean Masks Derived from ESA CCI Water Bodies v4.0 (Version 1.0) [dataset], GFZ Data Services, https://doi.org/10.5880/G3P.2025.001, 2025a.

Sharifi, E., Haas, J., Boergens, E., Dobslaw, H., and Güntner, A.: Technical note: GRACE-compatible filtering of water storage data sets via spatial autocorrelation analysis, Hydrol. Earth Syst. Sci., 29, 6985-6998, https://doi.org/10.5194/hess-29-6985-2025, 2025b.

Shihora, L., Balidakis, K., Dill, R., Dahle, C., Ghobadi-Far, K., Bonin, J., and Dobslaw, H.: Non-Tidal Background Modeling for Satellite Gravimetry Based on Operational ECWMF and ERA5 Reanalysis Data: AOD1B RL07, J. Geophys. Res.-Solid Earth, 127, https://doi.org/10.1029/2022jb024360, 2022.

Sindico, F., Hirata, R., and Manganelli, A.: The Guarani Aquifer System: From a Beacon of hope to a question mark in the governance of transboundary aquifers, Journal of Hydrology-Regional Studies, 20, 49-59, https://doi.org/10.1016/j.ejrh.2018.04.008, 2018.

Springer, A., Lopez, T., Owor, M., Frappart, F., and Stieglitz, T.: The Role of Space-Based Observations for Groundwater Resource Monitoring over Africa, Surveys in Geophysics, 44, 123-172, https://doi.org/10.1007/s10712-022-09759-4, 2023.

Strassberg, G., Scanlon, B. R., and Chambers, D.: Evaluation of groundwater storage monitoring with the GRACE satellite: Case study of the High Plains aquifer, central United States, Water Resources Research, 45, W05410, https://doi.org/10.1029/2008wr006892, 2009.

Strassberg, G., Scanlon, B. R., and Rodell, M.: Comparison of seasonal terrestrial water storage variations from GRACE with groundwater-level measurements from the High Plains Aquifer (USA), Geophysical Research Letters, 34, L14402, https://doi.org/10.1029/2007GL030139, 2007.

Swenson, S., Chambers, D., and Wahr, J.: Estimating geocenter variations from a combination of GRACE and ocean model output, J. Geophys. Res.-Solid Earth, 113, https://doi.org/10.1029/2007jb005338, 2008.

Takala, M., Luojus, K., Pulliainen, J., Derksen, C., Lemmetyinen, J., Kärnä, J. P., Koskinen, J., and Bojkov, B.: Estimating northern hemisphere snow water equivalent for climate research through assimilation of space-borne radiometer data and ground-based measurements, Remote Sensing of Environment, 115, 3517-3529, https://doi.org/10.1016/j.rse.2011.08.014, 2011.

Tapley, B. D.: Fundamentals of orbit determination, in: Theory of Satellite Geodesy and Gravity Field Determination, edited by: Sanso, F., and Rummel, R., Springer Lecture Notes in Earth Sciences, Springer, Berlin, Heidelberg, New York, 235-260, 1989.

Tapley, B. D., Bettadpur, S. V., Ries, J. C., Thompson, P. F., and Watkins, M. M.: GRACE measurements of mass variability in the Earth system, Science, 305, 503-505, https://doi.org/10.1126/science.1099192, 2004.

Taylor, R. G., Scanlon, B., Doll, P., Rodell, M., van Beek, R., Wada, Y., Longuevergne, L., Leblanc, M., Famiglietti, J. S., Edmunds, M., Konikow, L., Green, T. R., Chen, J. Y., Taniguchi, M., Bierkens, M. F. P., MacDonald, A., Fan, Y., Maxwell, R. M., Yechieli, Y., Gurdak, J. J., Allen, D. M., Shamsudduha, M., Hiscock, K., Yeh, P. J. F., Holman, I., and Treidel, H.: Ground water and climate change, Nature Climate Change, 3, 322-329, https://doi.org/10.1038/nclimate1744, 2013.

Tsypin, M., Cacace, M., Guse, B., Lischeid, G., Güntner, A., and Scheck-Wenderoth, M.: Damped groundwater response to recharge: From spectral analysis to regional modeling, J. Hydrol., 658, https://doi.org/10.1016/j.jhydrol.2025.133193, 2025.

Van der Knijff, J. M., Younis, J., and De Roo, A. P. J.: LISFLOOD: a GIS-based distributed model for river basin scale water balance and flood simulation, International Journal of Geographical Information Science, 24, 189-212, https://doi.org/10.1080/13658810802549154, 2010.

van Dijk, A. I. J. M., Renzullo, L. J., Wada, Y., and Tregoning, P.: A global water cycle reanalysis (2003-2012) merging satellite gravimetry and altimetry observations with a hydrological multi-model ensemble, HESS, 18, 2955-2973, 10.5194/hess-18-2955-2014, 2014.

Venäläinen, P., Luojus, K., Lemmetyinen, J., Pulliainen, J., Moisander, M., and Takala, M.: Impact of dynamic snow density on GlobSnow snow water equivalent retrieval accuracy, Cryosphere, 15, 2969-2981, https://doi.org/10.5194/tc-15-2969-2021, 2021.

Vreugdenhil, M., Greimeister-Pfeil, I., Preimesberger, W., Camici, S., Dorigo, W., Enenkel, M., van der Schalie, R., Steele-Dunne, S., and Wagner, W.: Microwave remote sensing for agricultural drought monitoring: Recent developments and challenges, Frontiers in Water, 4, https://doi.org/10.3389/frwa.2022.1045451, 2022.

Wang, T. J., Franz, T. E., You, J. S., Shulski, M. D., and Ray, C.: Evaluating controls of soil properties and climatic conditions on the use of an exponential filter for converting near surface to root zone soil moisture contents, J. Hydrol., 548, 683-696, https://doi.org/10.1016/j.jhydrol.2017.03.055, 2017.

Weise, K., Höfer, R., Franke, J., Guelmami, A., Simonson, W., Muro, J., O'Connor, B., Strauch, A., Flink, S., Eberle, J., Mino, E., Thulin, S., Philipson, P., van Valkengoed, E., Truckenbrodt, J., Zanderg, F., Sánchez, A., Schröder, C., Thonfeld, F., Fitoka, E., Scott, E., Ling, M., Schwarz, M., Kunz, I., Thümer, G., Plasmeijer, A., and Hilarides, L.: Wetland extent tools for SDG 6.6.1 reporting from the Satellite-based Wetland Observation Service (SWOS), Remote Sensing of Environment, 247, https://doi.org/10.1016/j.rse.2020.111892, 2020.

Wendland, E. C., Rabelo, J. L., and Roehrig, J.: Guarani Aquifer System – The Strategical Water Source In South America, Institut für Tropentechnologie, 2006.

WGMS: Fluctuations of Glaciers (FoG) Database [dataset], https://doi.org/10.5904/wgms-fog-2025-02b, 2023.

WMO: The 2022 GCOS Implementation Plan (GCOS-244), World Meteorological Organization (WMO); United Nations Environment Programme (UNEP); International Science Council (ISC); Intergovernmental Oceanographic Commission of the United Nations Educational, Scientific and Cultural Organization (IOC-UNESCO), Geneva, 2022.

Wouters, B., Gardner, A. S., and Moholdt, G.: Global Glacier Mass Loss During the GRACE Satellite Mission (2002-2016), Frontiers in Earth Science, 7, https://doi.org/10.3389/feart.2019.00096, 2019.

Xu, L., Ferris, D., Huggins, X., Wong, J. S., Mohan, C., Sadri, S., Chandanpurkar, H. A., Sanyal, P., and Famiglietti, J. S.: From coarse resolution to practical solution: GRACE as a science communication and policymaking tool for sustainable groundwater management, J. Hydrol., 623, https://doi.org/10.1016/j.jhydrol.2023.129845, 2023.

Yao, F. F., Livneh, B., Rajagopalan, B., Wang, J. D., Crétaux, J. F., Wada, Y., and Berge-Nguyen, M.: Satellites reveal widespread decline in global lake water storage, Science, 380, 743-749, 10.1126/science.abo2812, 2023.

Zemp, M. and Welty, E.: Temporal downscaling of glaciological mass balance using seasonal observations, Journal of Glaciology, https://doi.org/10.1017/jog.2023.66, 2023.

Zemp, M., Jakob, L., Brun, F., and Sutterley, T.: Glacier monitoring from space is crucial, and at risk, EOS, 106, https://doi.org/10.1029/2025EO250290, 2025.

Zemp, M., Huss, M., Eckert, N., Thibert, E., Paul, F., Nussbaumer, S. U., and Gärtner-Roer, I.: Brief communication: Ad hoc estimation of glacier contributions to sea-level rise from the latest glaciological observations, Cryosphere, 14, 1043-1050, https://doi.org/10.5194/tc-14-1043-2020, 2020.

Zemp, M., Huss, M., Thibert, E., Eckert, N., McNabb, R., Huber, J., Barandun, M., Machguth, H., Nussbaumer, S. U., Gartner-Roer, I., Thomson, L., Paul, F., Maussion, F., Kutuzov, S., and Cogley, J. G.: Global glacier mass changes and their contributions to sea-level rise from 1961 to 2016, Nature, 568, 382-+, https://doi.org/10.1038/s41586-019-1071-0, 2019.

Zhang, J., Liesch, T., and Goldscheider, N.: Impacts of climate change and human activities on global groundwater storage from 2003 to 2022, J. Hydrol., 664, 134298, https://doi.org/10.1016/j.jhydrol.2025.134298, 2026.